molecular pharmaceutics

Article

pubs.acs.org/molecularpharmaceutics

Two-Stage Desorption-Controlled Release of Fluorescent Dye and Vitamin from Solution-Blown and Electrospun Nanofiber Mats Containing Porogens

S. Khansari,[†,⊥] S. Duzyer,[‡,⊥] S. Sinha-Ray,[†] A. Hockenberger,[‡] A. L. Yarin,*[,†,§] and B. Pourdeyhimi[∥]

[†]Department of Mechanical and Industrial Engineering, University of Illinois at Chicago, 842 West Taylor Street, Chicago, Illinois 60607-7022, United States

[‡]Faculty of Engineering, Textile Engineering Department, Uludag University, Bursa 16059, Turkey

[§]College of Engineering, Korea University, Seoul, South Korea

[∥]The Nonwovens Institute, Box 8301, North Carolina State University, Raleigh, North Carolina 27695-8301, United States

ABSTRACT: In the present work, a systematic study of the release kinetics of two embedded model drugs (one completely water soluble and one partially water soluble) from hydrophilic and hydrophobic nanofiber mats was conducted. Fluorescent dye Rhodamine B was used as a model hydrophilic drug in controlled release experiments after it was encapsulated in solution-blown soy-protein-containing hydrophilic nanofibers as well as in electrospun hydrophobic poly(ethylene terephthalate) (PET)-containing nanofibers. Vitamin B_2 (riboflavin), a partially water-soluble model drug, was also encapsulated in hydrophobic PET-containing nanofiber mats, and its release kinetics was studied. The nanofiber mats were submerged in water, and the amount of drug released was tracked by fluorescence intensity. It was found that the release process saturates well below 100% release of the embedded compound. This is attributed to the fact that desorption is the limiting process in the release from biopolymer-containing nanofibers similar to the previously reported release from petroleum-derived polymer nanofibers. Release from monolithic as well as core−shell nanofibers was studied in the present work. Moreover, to facilitate the release and ultimately to approach 100% release, we also incorporated porogens, for example, poly(ethylene glycol), PEG. It was also found that the release rate can be controlled by the porogen choice in nanofibers. The effect of nanocracks created by leaching porogens on drug release was studied experimentally and evaluated theoretically, and the physical parameters characterizing the release process were established. The objective of the present work is a detailed experimental and theoretical investigation of controlled drug release from nanofibers facilitated by the presence of porogens. The novelty of this work is in forming nanofibers containing biodegradable and biocompatible soy proteins to facilitate controlled drug release as well as in measuring detailed quantitative characteristics of the desorption processes responsible for release of the model substance (fluorescent dye) and the vitamin (riboflavin) in the presence of porogens.

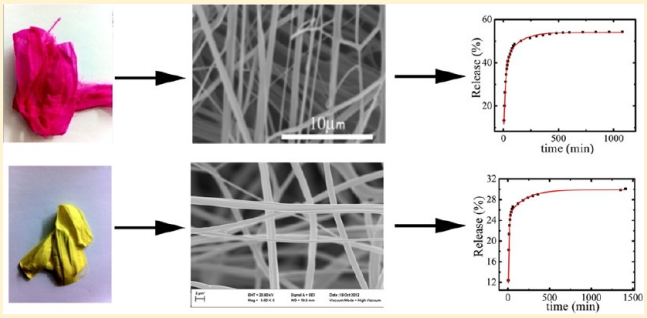

KEYWORDS: *controlled release, nanofibers, soy protein, porogens, desorption*

INTRODUCTION: BACKGROUND AND MOTIVATION

Recent developments for maintaining damaged or diseased tissues involve biodegradable and biocompatible scaffolds.[1−4] The main aim in the development of tissue scaffolds is to produce a material that resembles native extracellular matrix (ECM) in its physical and biological structure as well as chemical composition.[5] Engineered tissue scaffolds provide a temporary base for cells until the ECM is regenerated or repaired.[6−8] An important feature of native ECM is its nanoscaled structure. Collagen fibers in typical tissues range from 10 to a few hundred nanometers (cross-sectional diameter) and form a nonwoven nanofibrous matrix.[9] Cell behavior and activity is directly affected by the size of the scaffold fibers.[10−12] The nanoscaled texture of native tissues is of great importance for engineered tissues, such as blood vessel tissues. As discussed in ref 13, the nanoscaled network structure of bacterial cellulose has shown promising results as a substrate for regeneration of a wide range of tissues including skin. Therefore, cellulose nanofibrous networks are being widely investigated for wound-dressing purposes. Higher cell adhesion is reported for fibers with sizes smaller than that of the actual cells. As a result of better cell adhesion, their activity improves.[14] In ref 10, it was shown that osteoblasts and osteoclasts, which are bone-forming and -resorbing cells, revealed higher functionality to spherical nanophase alumina particles with an average grain size less than 100 nm compared to alumina particles larger than 100 nm. Alumina is widely used in

Received: June 12, 2013
Revised: September 8, 2013
Accepted: November 5, 2013
Published: November 5, 2013

orthopedic and dental treatments. Electrospun polycaprolactone (PCL) nanofiber mesh was reported to resemble native ECM in rat's cornea.[5]

Biocompatibility of engineered tissues is an important issue in order to suppress major immune response resulting from incompatibility with the host tissue. Porosity is another major factor required for the smooth and fast transfer of nutrients as well as cell attachment and activity. Biodegradability is still another critical feature required for implanted tissue scaffolds so that another surgery is not needed to remove them after the injured tissue is repaired.[6−8,15]

Biopolymer nanofibers have been utilized in cartilage and bone tissues.[4,12,16,17] Natural materials such as silk, chitosan, and dextran have been electrospun and functionalized as tissue scaffolds.[18,19] Silk fibers have been successfully utilized for bone marrow stem cell attachment and growth.[18] To enhance further tissue functionalization and its biocompatibility as well as cell adhesion to them, multilayered nanofiber mats have been used as scaffolds. For instance, collagen types I and III nanofibers were collected as layered mats so that the scaffold structure would closely resemble native ECM.[20,21]

Production of compound biopolymer nanofibers with distinct degradation times of the components is another method to improve cell attachment and in-growth. When one biopolymer degrades much faster than the other one in the scaffold, it produces voids ranging from a few hundred nanometers to micrometer size in the tissue structure. That brings about additional cell adhesion to the fibrous mesh. As shown in ref 22, PCL and gelatin nanofibers result in an enhanced porous structure because of the fast degradation of gelatin.

Biomaterials such as polymer nanofibers, which possess a high surface area/volume ratio, hold great potential as drug carriers. Drug delivery through biopolymers is attractive because they are capable of efficient delivery of a drug to a specified type of cell or compartment in the body.[23] Moreover, in many cases, drug delivery should be combined with the implanting of biodegradable scaffolds for disinfection and repairing of diseased or injured tissue. In general, a smaller size drug carrier increases the rate of drug delivery to the body and consequently enhances drug absorbance in a specified target. Several drugs have been delivered in controlled-release processes from nanofibrous scaffolds.[5,24] In ref 25, tetracycline hydrochloride was released from poly(ethylene-*co*-vinylacetate) (PEVA) nanofibers, poly(lactic acid) (PLA) nanofiber mesh, or their 50:50 wt % blend. Also, poly(lactic acid) nanofiber mats were used for loading the antibiotic drug Mexofin, which prevents surgery-induced adhesions.

Typically, to produce nanofibers for use as drug carriers, a drug is premixed with the carrier polymer solution from which the fibers are formed. After the fibers have been formed, drug nanoparticles may be exposed at the nanofiber surface. In some cases, drugs are dispersed in the solution and the resulting nanofibers as a molecular dispersion. It is also possible to encapsulate drugs inside nanofibers.[3]

The main goal of controlled drug delivery is to optimize the release profile and to minimize side effects by targeting specific cells or tissues and enhancing compatibility of drug with human body.[16,26,27] Targeted deliveries are advantageous specifically for highly toxic drugs such as anticancer agents.[28,29] Biocompatible and/or biodegradable polymers were used for controlled drug delivery in refs 30 and 31, and several biopolymers are discussed as perspective drug carriers in refs 5, 14, and 17. As reported in ref 32, the first commercial product for controlled drug delivery from biodegradable polymers introduced in 1989 had the trade name 'Lupron Depot'. This product was leuprolide encapsulated in poly(D,L-lactide-co-glycolide) (PLGA) microspheres.

Several models have been proposed for controlled drug delivery.[33−37] In general, drug delivery is associated with diffusion, desorption, chemical reaction (or solvent activation), and transport.[35] In the case of drug release from nondegradable polymer nanofibers, the dominant mechanism was shown to be desorption.[36,37] The mechanisms responsible for drug delivery from biodegradable polymers are diffusion, osmosis, and polymer degradation.[32]

Monolithic and core−shell nanofiber mats hold great promise for biomedical applications. Controlled drug release from such nanofibers was studied in refs 25, and 36−40. In particular, it was shown that core−shell nanofibers loaded with drug or dye in the core reveal a reduced release. To facilitate the release of an encapsulated material from the nanofiber core, a compound leachable in water (a porogen; i.e., a pore promoter) can be added to the shell, which helps to expose the drug or dye embedded in the core to the surrounding medium. As a porogen, a nontoxic poly(ethylene glycol), PEG, M_w = 10 kDa, was blended with the other fiber-forming polymers.[41] Using nondegradable nanofibers without porogens, much less than 100% of the dye/drug was released, which was attributed to desorption being the limiting mechanism of the release process in refs 36 and 37.

So far, only nanofibers formed by electrospinning have been used in controlled drug delivery. Electrospinning is a relatively slow process. There are other processes that can form nanofibers at a much higher rate, for example, solution blowing.[42] This method employs high-speed air as a driving force to blow polymer-solution jets into nanofibers. Monolithic as well as core−shell nanofibers can be formed by solution blowing.[42] Moreover, this method has been already applied to form biocompatible and biodegradable soy-protein-containing solution-blown nanofiber mats.[43,44]

In addition to biocompatible scaffolds, significant efforts have been aimed at the development of biocompatible and biodegradable sutures, for which soy protein seems to be an attractive candidate.[45] However, the problem with the available soy-protein-based sutures is their low strength.[46] Moreover, the available methods of manufacturing soy-based sutures involve extrusion at high temperature, which excludes the possibility of loading the raw material with drugs that can facilitate healing. In this regard, isothermal solution blowing, demonstrated in refs 42−44, holds great promise for biomedical sutures.

Poly(ethylene terephthalate) (PET)-based materials are widely used as surgical sutures and meshes owing to their physical and chemical properties.[47−51] PET is a semiaromatic polyester that possesses good mechanical and thermal properties. Because it can form fibers, it is widely used in the textile industry. Fibers made of PET are nonbiodegredable, nontoxic, and noncancerogenous, which has resulted in the wide use of PET as surgery sutures, medical gowns, ligaments and vessel grafts as well as hospital sheets in the form of yarns and fabrics.[52−56]

In drug-delivery systems and tissue-engineering applications, material selection, determined by desirable chemical, interfacial, and biological functions, plays a key role.[57] Biodagredable or nonbiodegredable polymers can be used, depending on the application area. Although many processes aimed at the use of biodegradable polymers, in some cases biodegredable polymers are not necessarily needed. During the repair process of blood vessels, bone, skin, and soft tissue or the replacement of the

damaged tissue with the scaffold, a stable, biocompatible material with good mechanical properties is required. The latter implies nonbiodegradable polymers. This is the reason that applications of inexpensive and biocompatible PET proliferated well beyond the initial usage as artificial blood vessels.

In the present work, PET was chosen because it is a nontoxic, noncancerogenous material with good mechanical properties. PET is hydrophobic, and its free surface energy is low. Therefore, some additives (porogens) were added to PET solution to facilitate the controlled release of riboflavin. This study is a step toward the controlled release of anticancer drugs. During the treatment of cancer patients, an anticancer drug can be administered orally or systemically by injection, even though the drug will reach a targeted organ at a lower dose because it is spread to the other organs, which is disadvantageous. Therefore, patients are given a higher dose of drugs, which results in many side effects.[58] For an effective cancer treatment after surgery, drug-loaded nanofiber mats can be applied to the operated areas to improve the healing.[58−60] Thus, side effects and spreading of cancer (metastasis) will be lowered, and possible additional surgical intervention and overdose drug administration to the patient will be prevented. For instance, especially in brain tumor surgeries, PET nanofiber mats can be implanted into the operated area after the removal of the tumor. Because this structure should meet the desired requirements associated with mechanical properties, toxicology, and biocompatibility, nonbiodegredable PET is preferrable to facilitate controlled drug release.

Electrospun PET nanofiber mats are attractive for drug delivery because electrospinning allows the nanofiber mat to be functionalized at room temperature.[47] In practice, the drugs intended for controlled release can be either completely or partially soluble in the solvent of the host polymer, resulting in variations of surface compatibility. Drug release can be modulated by the choice of porogens. To the best of our knowledge, no in-depth studies on the effect of porogens on the release kinetics have been conducted.

In the present work, two systems were studied. The first one is soy-protein-containing nanofibers with embedded Rhodamine B, a model drug that is readily soluble in the solvent and aqueous media. These nanofibers were formed by solution blowing using the host−guest approach, with nylon 6 or PVA being the host polymers and soy protein being the guest biopolymer. This choice was made judiciously because both host polymers selected are used as biologically safe and proven biomaterials.[61,62] The second system explored is PET-based nanofibers loaded with Rhodamine B or riboflavin. Riboflvin is used as a model drug that is poorly soluble in the solvent and aqueous media. Riboflavin and Rhodamine B were separately premixed with the polymeric solutions. Then, riboflavin- and Rhodamine B-containing PET-based nanofiber mats were formed by electrospinning. The release kinetics of model drugs from both systems was studied, which is the main aim of the present work.

EXPERIMENTAL SECTION

Materials. Protein isolate PRO-FAM 955 (SP 955) was received from ADM Specialty Food Ingredients. Polyamide 6 (nylon 6) (M_w = 65.2 kDa) was supplied by BASF. Formic acid (>95%), trifluoroacetic acid, TFA (ReagentPlus 99%), chloroform (anhydrous, ≥99%), poly(ethylene glycol) with an average molecular weight of 3400 Da, riboflavin (≥98%), and rhodamine B fluorescent dye were purchased from Sigma-Aldrich. Additionally, poly(ethylene oxide) (PEO) with three different average molecular weights (200, 400, and 600 kDa) was purchased from Sigma-Aldrich. Poly(vinyl alcohol) (88 mol %, hydrolyzed) ~78 kDa was supplied by Polysciences, Inc. Poly(ethylene terephthalate) (PET) (granular) was provided by NC State University. All products were utilized without any postprocessing or further treatment.

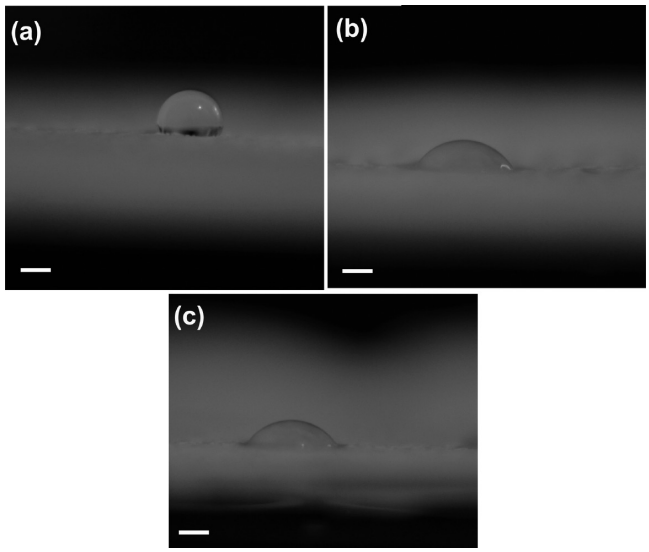

Figure 1. Water droplet softly deposited on (a) PET, (b) PET/PEG, and (c) PET/PEG/PEO (M_w 400 kDa). The scale bars are 1 mm.

Solution Preparation. As in refs 43 and 44, a blend of soy protein/nylon 6 (50:50 w/w) was prepared, with 1.5 g of SP 955 being mixed with 9.5 g of formic acid and stirred on a hot plate at 75 °C for 24 h. After that, 1.5 g of nylon 6 was added to this solution, and the solution was stirred on the hot plate for another 24 h at the same temperature. Then, 0.03 g of Rhodamine B was added to the prepared blend, and the vial containing the solution was completely wrapped with aluminum foil to prevent its exposure to light. The soy protein/nylon 6 solution containing Rhodamine B was sonicated for 30 min to mix completely the dye in the solution.

Also, two blends of soy protein/nylon 6 (50:50 w/w) were produced as described above, and PEG was added to both of them. PEG content was 5 w/w PEG/soy protein and nylon 6 in one blend and 10 w/w PEG/soy protein and nylon 6 in another blend. After adding PEG, the samples were left on the hot plate for 30 min under stirring to mix completely. The last step was to cover the vials with aluminum foil and add 0.03 g of Rhodamine B to each solution. The samples were then sonicated for 30 min to form a homogeneous solution.

A solution of nylon 6 in formic acid was prepared as follows. Nylon 6 (2.0 g) was added to 10.0 g of formic acid and left on the hot plate at 75 °C for 1 day. After that, 0.02 g of Rhodamine B was added to this solution and sonicated for 30 min.

To produce core−shell nanofibers, the core and shell solutions were prepared as follows. The core solution consisted of 1.3 g of SP 955 mixed with 8.7 g of formic acid for 24 h at 75 °C. Then, 1.0 g of nylon 6 was mixed with this blend. Finally, 0.023 g of Rhodamine B was added to the core solution, and the vial was wrapped with aluminum foil to prevent light exposure. The shell solution was a blend of 20 wt % nylon 6 in formic acid with no Rhodamine B added. To examine the effect of PEG as the leachable polymer (porogen) on the drug-release kinetics from core−shell nanofibers, two additional shell solutions were prepared: a 20 wt % nylon 6 solution in formic acid was used

dx.doi.org/10.1021/mp4003442 | Mol. Pharmaceutics 2013, 10, 4509−4526

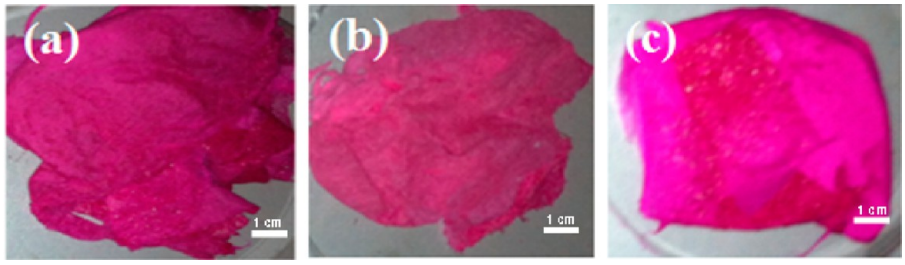

Figure 2. Rhodamine B-containing nanofiber mats. (a) Monolithic soy protein/nylon 6 (50:50 w/w) with 1 wt % Rhodamine B. (b) Core−shell soy protein-containing nanofiber mat with 1 wt % dye premixed with the solution and blown into the fiber core. Some dye diffused from the core to the shell when both were still liquid, which explains the pink color of the mat. (c) Monolithic soy protein/PVA (50:50 w/w) nanofibers with 2.5 wt % Rhodamine B.

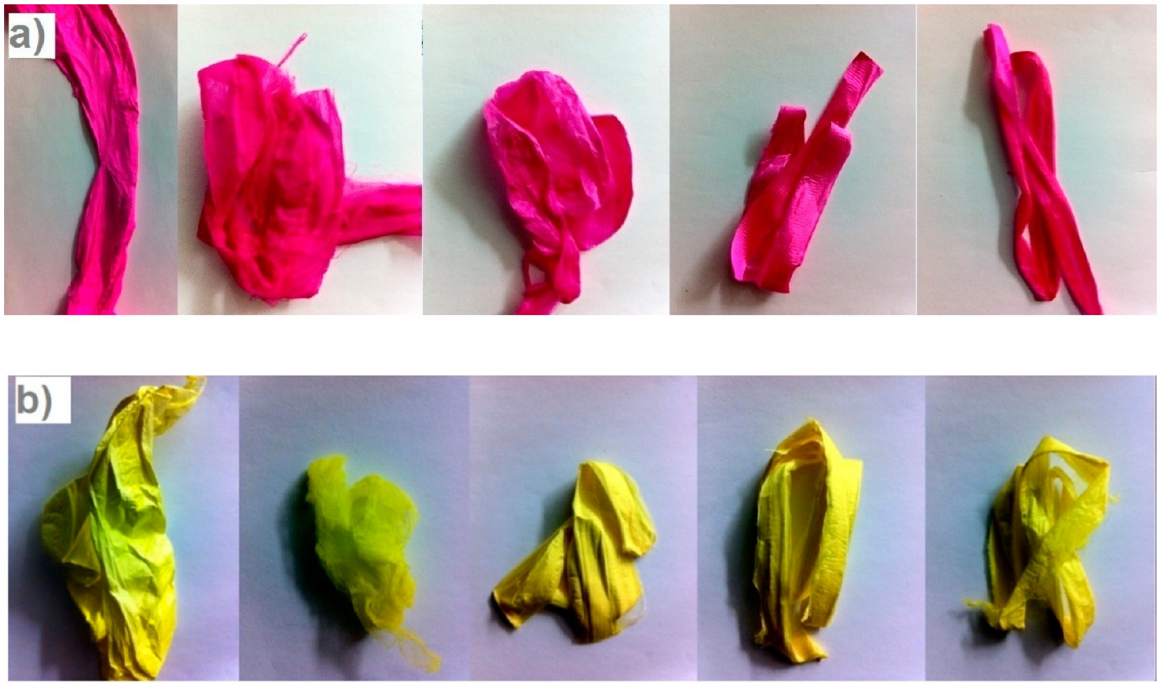

Figure 3. (a) Rhodamine B-containing nanofiber mats I1, J1, K1, L1, and M1 (from left to right, respectively). (b) Riboflavin- containing nanofiber mats I2, J2, K2, L2, and M2 (from left to right, respectively).

as a base, and 5 wt % PEG/nylon 6 and 10 wt % PEG/nylon 6 were prepared from it and left on the hot plate at 75 °C for 30 min to mix completely. Note that the latter two solutions were used as a nanofiber PEG-containing shell, whereas the core solutions were prepared as described above.

In addition, a solution of soy protein with poly(vinyl alcohol) (PVA) was prepared, with the SP/PVA ratio being 50:50 w/w. First, 0.8 g of soy protein was mixed with 9.5 g of formic acid for 1 day at 75 °C. Then, 0.8 g of PVA was added to the solution, and the solution was kept under stirring for another day. After that, 0.04 g of Rhodamine B was added to the solution. The blend of SP/PVA with Rhodamine B was left under stirring for 30 min at room temperature fully protected from light.

A solution of 15 wt % PET was prepared by mixing 1.5 g of PET with 8.5 g of solvent consisting of 50 wt % TFA and 50 wt % chloroform. The solution was kept at 55 °C on the hot plate for 4 h. Then, 0.03 g of Rhodamine B was added to the homogeneous solution and sonicated for 30 min to mix properly.

To prepare the PET/PEG solution, a 15 wt % PET solution in TFA/chloroform was prepared as explained above. Next, 0.15 g of PEG was added, and the solution was mixed for 30 min using magnetic stirring at 55 °C on the hot plate. Finally, 0.03 g of Rhodamine B was added and sonicated for 30 min.

A solution of PET/PEG/PEO was prepared by adding 0.15 g of PEO to the above-mentioned PET/PEG solution and mixing on the hot plate for 1 h at 55 °C. Three different solutions of this type were prepared with various molecular weights of PEO (i.e., 200, 400, and 600 kDa). In this case, PEG and PEO were used as two different leachable polymers (porogens). At the end, 0.03 g of Rhodamine B was mixed with each solution and left to sonicate for 30 min.

To prepare riboflavin-containing solutions, PET-based solutions were prepared as explained above. In each case, instead of Rhodamine B, 0.03 g of riboflavin was mixed and sonicated for 30 min. Note that all of the Rhodamine B- and riboflavin-containing solutions were wrapped with aluminum foil to prevent light exposure.

Surface Energy. To evaluate the surface energy of the water−sample interaction, the following experiments were conducted. Pure and blend polymer solutions were cast and dried on a glass slide. After that, a single water droplet was softly deposited on the cast material, as shown in Figure 1. Contact angle measurement to characterize the surface energy on cast

dx.doi.org/10.1021/mp4003442 | *Mol. Pharmaceutics* 2013, 10, 4509−4526

materials is preferable compared to measurements on nanofiber mats because the latter contain about 90% porosity, which, in some cases, makes them act as almost superhydrophobic, whereas the polymer material itself can be rather hydrophilic.[63,64] The results in the present work show that water droplets spread immediately on all pure soy-protein-containing films, which clearly shows that the surface energy of such materials is high. The other polymers blended to form soy-protein-based nanofibers in the present work were nylon 6, PEG, PVA, and PEO. These polymers are also highly polar and thereby facilitate the spreading of water droplets.[65] However, water droplets did not spread on the PET-based systems. It can be seen that on the PET film the contact angle is 125° (Figure 1a) and on the PET/PEG film (Figure 1b) the contact angle is 45°, whereas on the PET/PEG/PEO (M_w = 400 kDa) films the contact angle is 52° (Figure 1c). The results show that the addition of these porogens to PET facilitates water interaction with the PET-based nanofiber mats as well as yields a higher release percentage compared to the pure PET-based nanofiber mats, as the results discussed below show. For comparison, note that the contact angle of water droplets on PET nanofiber mats is about 142.5° because of the presence of air in the interfiber pores; on PET/PEG nanofibers with the embedded riboflavin, the contact angle diminishes to approximately 75°.

The energy of the dye− or drug−polymer interactions was characterized by the desorption enthalpy measured and is listed in the Results and Discussion section. Note that a higher desorption enthalpy diminishes the dye- or drug-release rate because the binding energy is higher in such cases.

Solution Blowing. Solution blowing was used to produce nanofibers from the above-mentioned solutions following the methods outlined in refs 42−44. A 13 G needle made of stainless steel was used to issue a solution when monolithic nanofibers were formed. At the end of the needle, the solution was entrained by the coaxial high-speed air jet with an upstream pressure of about 30 psi. The solution flow rate was kept at 4.0 mL/h. As a result, a solution jet was formed, stretched and underwent bending instability because of the air jet surrounding the needle. Consequently, continuous monolithic nanofibers were produced.

To form core−shell nanofibers, the core solution was issued through a 18 G stainless steel needle, whereas the shell solution was supplied through a 13 G needle, both at a 3 mL/h flow rate. The 18 G needle issuing the core solution was located coaxially inside the needle that was delivering the shell solution. The core−shell polymer jet was entrained by a coaxial high-speed air stream similar to the approach for forming monolithic fibers. As a result, the core containing soy protein was encapsulated by a nylon 6 shell, and core−shell nanofibers were formed. Both monolithic and core−shell nanofibers were produced at room temperature and humidity. They were collected under reduced light to diminish the light exposure of dye-containing nanofibers and kept in an enclosure totally protected from light.

Nanofibers were collected on a rotating drum covered with an aluminum foil that was kept at a distance of 15−19 cm below the needle. The collected Rhodamine B-containing monolithic nylon 6 nanofibers are denoted as sample A, monolithic SP/nylon 6 (50:50 w/w) nanofibers, sample B, monolithic SP/PVA (50:50 w/w), sample C, monolithic SP/nylon 6 (50:50 w/w) + 5 wt % PEG nanofibers, sample D, monolithic SP/nylon 6 + 10 wt % PEG nanofibers, sample E, core−shell SP/nylon 6 nanofibers,sample F, core−shell SP/nylon 6 + 5 wt % PEG nanofibers, sample G, and core−shell SP/nylon 6 + 10 wt % PEG nanofibers, sample H. Several representative images of the collected nanofibers containing Rhodamine B are shown in Figure 2.

Electrospinning. For electrospinning of PET-based solutions, an electric potential difference of 15 kV was applied between the liquid drop at the needle exit and the grounded rotating-disc collector. The polymer solution was electrospun from a plastic syringe with an internal diameter of about 25 G at a flow rate of 1 mL/h. The fiber mats were collected in darkness to protect the fluorescent materials in the nanofiber mats from degradation. An image of the electrospun PET-based nanofiber mat loaded with Rhodamine B is shown in Figure 3a, and the image of the mat loaded with riboflavin is shown in Figure 3b. For the sake of brevity, the nanofiber mats formed from PET, PET/PEG, PET/PEG/PEO (200 kDa), PET/PEG/PEO (400 kDa), and PET/PEG/PEO (600 kDa) loaded with Rhodamine B are denoted as I1, J1, K1, L1, and M1, respectively. Similarly, nanofiber mats formed from PET, PET/PEG, PET/PEG/PEO (200 kDa), PET/PEG/PEO (400 kDa), and PET/PEG/PEO (600 kDa) loaded with riboflavin are denoted as I2, J2, K2, L2, and M2, respectively.

Release Experiments. All nanofiber mats with the embedded Rhodamine B fluorescent dye were cut into rectangular pieces weighing 5−10 mg and put into a glass vial containing 5 mL of deionized water. The vial was wrapped with aluminum foil to prevent any light exposure of the samples because of the sensitivity of the dye to light. In these experiments, dye was released from the nanofibers into water, and the fluorescence intensity of the water was measured periodically to evaluate the released amount of dye. To accomplish this, 200 μL samples of water with the released dye were periodically extracted from the vial and delivered into a well inside a 96-well microplate. Four wells were filled with the 200 μL samples simultaneously, and the fluorescence intensity of the dye present in water was measured using Gemini SpectraMax spectrofluorometer (Molecular Devices), with the excitation wavelength of 553 nm and the emission wavelength of 627 nm, appropriate for Rhodamine B.

Riboflavin-containing nanofiber mats underwent the release experiments according to the same protocol as described above for Rhodamine B. The only difference was the excitation wavelength of 268 nm and the emission wavelength of 373 nm, appropriate for riboflavin.

The average fluorescence intensity corresponding to the four wells was reported as the fluorescence intensity of Rhodamine B or riboflavin released during a certain time. Then, water in the vial was completely replenished. This process was periodically repeated in specified time intervals. The fluorescence intensity is proportional to the released mass in the water sample. Therefore, it was possible to record the mass of released fluorescent material (Rhodamine B or riboflavin) during a certain time interval and, as a result, to measure the cumulative mass released as a function of time. For each type of sample, release experiments were repeated three times with nanofiber mat samples cut from the same batch. All of the release experiments were conducted at room temperature.

Optical Observations. Scanning electron microscopy (SEM) observations for solution-blown samples were done using a Hitachi S-3000N variable-pressure SEM. Samples were sputter-coated with Pd/Pt up to 10 nm in thickness prior to scanning microscopy. The as-spun and immersed samples were observed. For electrospun samples, surface morphologies of nanofibers were observed using Carl Zeiss Evo 40.

■ RESULTS AND DISCUSSION

Effect of Immersion of Soy-Protein-Based Nanofiber Mats in Water. Weight-loss analysis was conducted for the dye-containing soy-protein-based nanofiber samples that were

dx.doi.org/10.1021/mp4003442 | Mol. Pharmaceutics 2013, 10, 4509−4526

Table 1. Average Weight Loss of the Soy-Protein-Based Nanofiber Samples

sample	average weight loss (%)	sample	average weight loss (%)
soy protein/nylon 6 50:50 w/w , monolithic nanofibers	11.56 ± 4.41	soy protein core−shell nanofobers	6.41 ± 2.06
soy protein/nylon 6 + 5 wt % PEG, monolithic nanofibers	22.00 ± 3.58	soy protein core−shell + 5 wt % PEG in shell nanofibers	13.29 ± 2.41
soy protein/nylon 6 + 10 wt % PEG, monolithic nanofibers	35.6 ± 6.39	soy protein core−shell + 10 wt % PEG in shell nanofibers	14.47 ± 1.94
soy protein/PVA 50:50 w/w, monolithic nanofibers	68.62 ± 9.34		

immersed in a water bath periodically during the dye-release experiments. According to ref 66, soy-protein-based nanofiber mats tend to lose weight in contact with water. In addition, for PEG-containing fibers, leaching of the porogen (PEG) into water was desirable. Note that a host polymer such as PVA is also expected to be dissolved in water. After the release process reached its final saturation, the mass loss of the samples was quantified as

$$L = \left(1 - \frac{W_2}{W_1}\right)100\% \quad (1)$$

where W_1 is the sample weight before the immersion in water and W_2 is the sample weight after the completion of the release process and full dry out.

The values of L are reported in Table 1 for all of the Rhodamine B-containing samples that underwent the release process, excluding the pure nylon 6 samples. Because nylon 6 is not soluble in water, almost no weight loss was observed in its samples.

Table 1 shows that the core−shell Rhodamine B-containing samples had the lowest value of the material loss because the water-soluble soy protein in the core was partially sheltered by water-insoluble nylon 6 in the shell. Table 1 also shows that PEG-containing samples revealed a higher weight loss compared to the monolithic soy protein/nylon 6 nanofibers, which stems from the high solubility of PEG in water. Soy protein/PVA nanofiber mats had the highest weight loss because of the high water solubility of PVA in addition to that of soy protein.

SEM images of nanofiber samples A, B, C, E, F, and H before and after immersion in water are shown in Figure 4a−f, respectively. The images show that the general morphology of the nanofibers does not change after immersion in water, with the exception of sample C. Figure 4c2 shows that after immersion in water, nanofiber mat C lost its fibrillar structure and turned into an almost solid block, which resulted from a partial dissolution of the constituent materials (soy protein and PVA). No images for samples D and G before and after the immersion are shown in Figure 4 because they contained the same materials as that in samples E and H, respectively, which have a larger content of PEG. Therefore, it was expected that changes in the general morphology of samples D and G after immersion in water would be less pronounced than those of samples E and H in Figure 4.

SEM images of samples I2, J2, K2, L2, and M2 are shown in Figure 5a−e, respectively. It can be seen that these fibers are larger in comparison to those in Figure 4. For the sake of brevity, SEM images of samples I1−M1 are not shown.

SEM images of samples I1 (containing Rhodamine B) and I2 (containing riboflavin) after the immersion in water are shown in Figure 6. It can be seen that even after the immersion in water there is no visible morphological changes in the sample I1 (Figure 6a) and the fibers stay smooth. However, there are visible striations on the fibers in sample I2 (Figure 6b). The striations appear because riboflavin is partially soluble in the solvent used to form nanofibers, and the blended riboflavin forms striations in the fibers (unlike Rhodamine B, which is readily soluble in the solvent). The release of riboflavin makes microcracks at the location of the striations, making them even more visible, as shown in Figure 6b. The presence of the striations also affects the riboflavin-release profile, as will be shown later. Similar striations were observed in riboflavin-loaded samples J2−M2. However, the visibility of the striations can be blurred because of the presence of porogens in the nanofibers. For the sake of brevity, they are not shown. It is emphasized that in the samples without riboflavin (A, B, C, E, F, H, and I1−M1) no striations were observed.

Release Experiments. The results on the kinetics of dye release from soy-protein-based nanofiber mats are shown in Figure 7. The figure demonstrates that the release process always saturates well below 100%. For every batch of samples, the release experiments were repeated at least three times, and the average release profiles are shown in Figure 7.

Figure 7a,b shows that the release process for pure nylon 6 nanofiber mats with 1 w/w dye/mat content saturated at a comparable release percentage as the soy protein/nylon 6 (50:50 w/w) fiber mat. For sample A, saturation of the dye-release process occurred at 58.93 ± 8.91%, and for sample B, at 60.12 ± 4.17%. Although the release saturation occurred at almost the same level, the saturation for sample B was reached at an earlier time in comparison to sample A. This is due to the fact that soy protein contains hydrophilic biopolymer chains that help to deliver water into the fiber bulk and thus enhance the release process from soy protein/nylon 6 nanofibers.

To enhance the dye-release process from soy-protein-containing nanofiber mats, PEG was used as a porogen in the samples with the expectation that because of its faster dissolution in water compared to soy protein the fibers with PEG will rapidly form nanopores after exposure to water. This should facilitate the release process. To demonstrate the effect of PEG, monolithic and core−shell soy protein/nylon 6 nanofibers were seeded with two different amounts of PEG (5 and 10 wt %). In Figure 7d,e, the release profiles for soy protein/nylon 6 (50:50 w/w) with 5 and 10% w/w PEG nanofibers are shown, respectively. It can be seen that a higher content of PEG in the samples results in a higher level of the ultimate release saturation for the PEG-containing fiber mats (Figure 7e) compared to the original soy protein/nylon 6 (50:50 w/w) fiber mats (cf. Figure 7b). Monolithic soy protein/nylon 6 nanofiber samples released dye up to 60.12 ± 4.17%. The addition of 5 w/w PEG/mat increased the release level up to 81.59 ± 3.75% for comparable soy protein/nylon 6 nanofiber samples, as seen in Figure 7d. For the 10% w/w PEG/mat, the ultimate release level approached 94.22 ± 1.33% in Figure 7e. The release process from monolithic soy protein/nylon 6 nanofibers saturated at about 1080 min (Figure 7b), whereas for the comparable samples with 10% w/w PEG, the active release process was much longer and saturated at about 10 270 min (Figure 7e).

The release profile for core−shell soy protein/nylon 6 nanofiber mats is illustrated in Figure 7f. In these fibers, the dye-containing core was surrounded by the nylon 6 shell. The

dx.doi.org/10.1021/mp4003442 | Mol. Pharmaceutics 2013, 10, 4509−4526

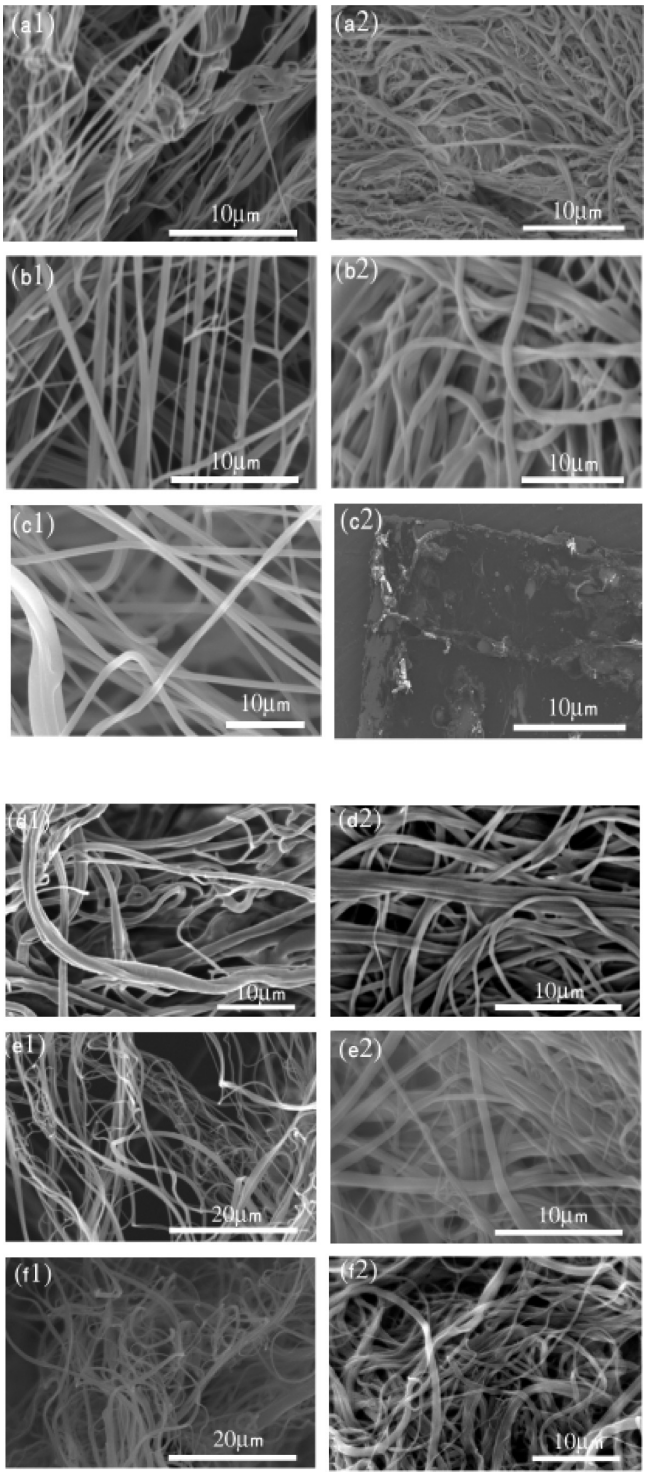

Figure 4. SEM images of dye-containing monolithic and core−shell nanofibers mats before and after immersion in water: sample (a) A, (b) B, (c) C, (d) E, (e) F, and (f) H. In all of the images, panels numbered 1 depict the dye-containing samples before the immersion in water, whereas panels numbered 2 depict the same samples after the immersion in water once the dye release had reached saturation.

lower saturation percentage for the core−shell nanofibers compared to that of soy protein/nylon 6 (50:50 w/w) nanofibers (cf. Figure 7, panels f and b) is easily noticeable. The soy protein/nylon 6 monolithic nanofiber samples reached the release saturation at 60.12 ± 4.17%, whereas for the soy protein/nylon 6 core−shell nanofiber samples the release saturated at 52.85 ± 3.49%. The nylon 6 shell, which is not water-soluble, hinders dye release from the core.

Figure 7c illustrates the dye-release process from soy protein/PVA (50:50) nanofiber mats. As the SEM image (Figure 4c) and Table 1 show, dissolution of the soy protein/PVA nanofibers in water is quite significant and is facilitated by the solubility of PVA and the hydrophilic nature of soy protein. As a result of the fiber material degradation in this case, the release process saturates at 78.32 ± 17.24% over a long period of time.

The presence of PEG in the shell of the core−shell fibers also facilitates dye release. Comparison of Figure 7, panels f−h demonstrates that a higher content of PEG in the shell (0, 5, and 10 wt %, respectively) facilitates the dye release from the core, increases the saturation level of the release process, and makes it longer. The release from core−shell soy protein/nylon 6 nanofiber mats saturated at 52.85 ± 3.49% (Figure 7f). When 5 wt % PEG was present in the shell, the saturation level increased to 58.28 ± 2.87% (Figure 7g), and at 10 wt % of PEG, the saturation level reached 63.48 ± 2.19% (Figure 7h).

The release kinetics of Rhodamine B from electrospun PET-based nanofiber mats (samples I1−M1) are illustrated in Figure 8. The dye release from pure PET nanofiber mats saturated at 2.1 ± 0.11% (Figure 8a). The encapsulation of PEG as a porogen in the PET-based nanofibers led to a significant boost in the release of Rhodamine B from the nanofibers. The dye-containing PET/PEG nanofiber mats revealed a 30.07 ± 1.03% level of release saturation (Figure 8b). The encapsulation of an additional porogen (i.e., PEO) in the PET/PEG nanofiber mats resulted in a lower level of release saturation. PET/PEG/PEO (200 kDa) nanofibers reached the ultimate saturation of 12.50 ± 1.87% (Figure 8c). The addition of the higher molecular weight PEO further reduced the ultimate release saturation value. In particular, the release from the monolithic electrospun PET/PEG/PEO (400 kDa) nanofibers saturated at 3.18 ± 0.21%, and the release from the PET/PEG/PEO (600 kDa) nanofibers saturated at 1.85 ± 0.15% (cf. Figure 8d,e, respectively).

The release kinetics of riboflavin from electrospun PET-based fibers with PEG and PEO encapsulated as porogens are illustrated in Figure 9. Riboflavin-containing nanofiber mats of pure PET revealed saturation of the release process at 3.99 ± 0.16% (Figure 9a). PET/PEG monolithic nanofiber mats loaded with riboflavin revealed release saturation at 10.23 ± 2.66% (Figure 9b). The presence of PEO in addition to PEG was detrimental and reduced the ultimate riboflavin release level to 7.35 ± 0.67% for PET/PEG/PEO (200 kDa), 5.55 ± 0.53% for PET/PEG/PEO (400 kDa), and 7.42 ± 0.55% for PET/PEG/PEO (600 kDa) (Figure 9c−e, respectively).

■ THEORETICAL VERSUS EXPERIMENTAL

Drugs embedded in nanofibers can be uniformly dispersed on the molecular level in the fiber bulk as well as at the free surfaces of the individual fibers, which include the outer cylindrical surface, the surfaces of all closed voids, and the interconnected pores with an outside opening. As was shown in the previous work of our group,[36] drug can be released from the nondegradable nanofibers only from the free surfaces that are connected to the surrounding medium, such as water (i.e., from the cylindrical outer surface and from the surfaces of the interconnected pores with the outside openings). The macroscopic manifestation of that fact is that the release process saturates at a release percentage well below 100%. This can happen only because the release process is driven by the desorption of the drug from the open surfaces rather than by solid-state diffusion. Indeed, solid-state diffusion, which is the

dx.doi.org/10.1021/mp4003442 | Mol. Pharmaceutics 2013, 10, 4509−4526

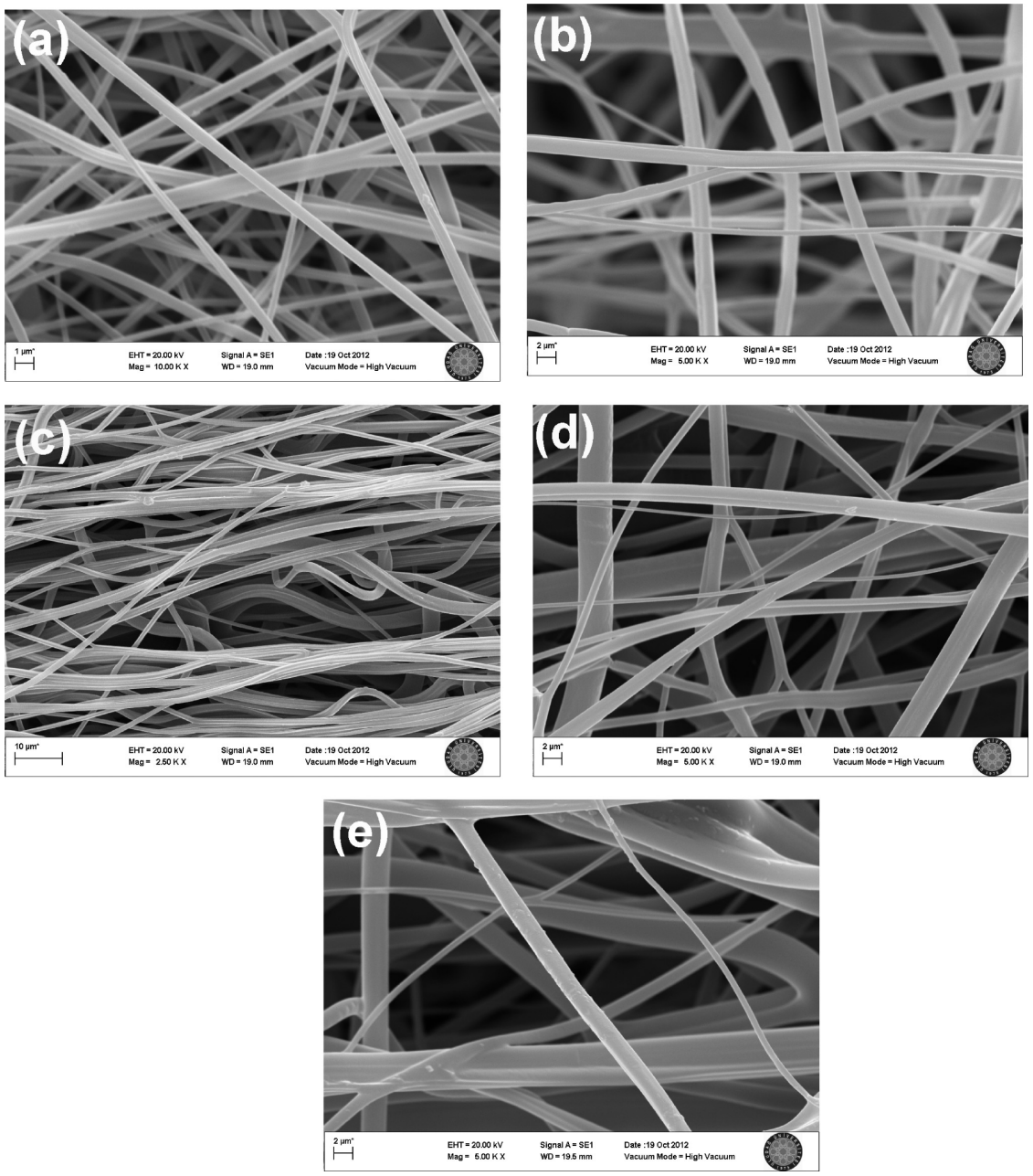

Figure 5. (a–e) SEM images of the electrospun samples I2–M2, respectively.

only process that could lead to a 100% release from the nondegradable nanofibers, is too slow and incommensurate with the overall duration of the release experiments.[36] To increase the release percentage from the nondegradable nanofibers as well as to manipulate the release kinetics, porogens are required, which, in fact, makes the nanofibers degradable and exposes new portions of drug to the environment during the release process. On the microscopic and nanoscopic levels, the presence of the interconnected pores with outside openings on the scale of several nanometers on nanofibers was demonstrated using SEM imaging in refs 67–69.

As reported in ref 70, the maximum solubility of Rhodamine dye in water is on the order of 0.1 wt %. Therefore, the maximum concentration of Rhodamine in water in the present experiments could not exceed 0.00002 wt %, and the maximum solubility of dye could not be reached in the release process. Therefore, the saturation of the release process seen in Figures 7 and 8 cannot be related to the maximum solubility of Rhodamine B dye in water and should be linked to the dye desorption from the nanopore surfaces in the individual nanofibers, as shown in ref 36. Higher-resolution SEM images of the individual solution-blown soy protein monolithic and core–shell nanofibers in ref 43 show that they contain multiple nanoscale pores. The pores perforate the entire nanofiber bulk. Most of the pores in the nanofibrous structure proliferate into the bulk from the nanofiber surface. Therefore, when such samples are immersed in water, nanopores are fully exposed to water and the dye desorption mechanism described in refs 36 and 37 is fully responsible for the release saturation seen in Figures 7a–h and 8a–e.

According to refs 36 and 37, dye release is a two-stage process. First, dye is released by desorption from the nanopore surfaces, which is a relatively slow, limiting stage of the dye/drug release. Then, the released dye is redistributed in water by diffusion, which is a very fast process comparatively. The saturation of the

dx.doi.org/10.1021/mp4003442 | *Mol. Pharmaceutics* 2013, 10, 4509–4526

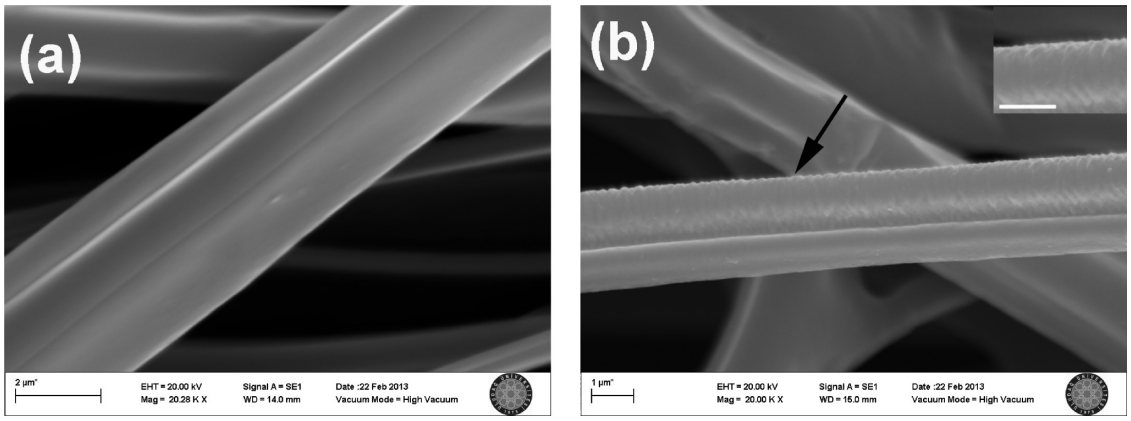

Figure 6. SEM images of the electrospun samples (a) I1 and (b) I2 after immersion in water. The arrow in panel b indicates the striations. A zoomed view of the striations is shown in the inset in panel b, and the scale bar in the inset is 1 μm.

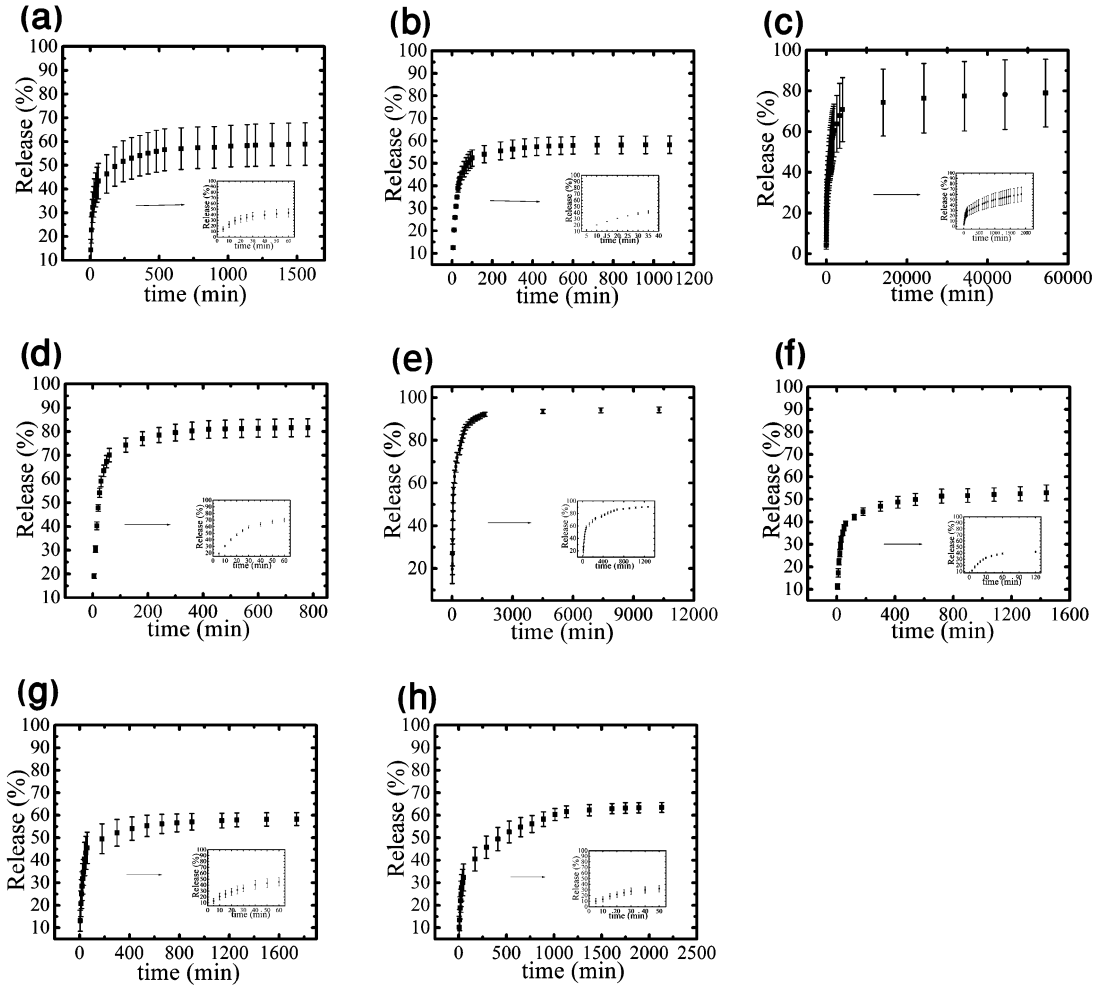

Figure 7. Average release profiles from solution-blown Rhodamine B-containing nanofiber mats: (a–h) samples A–H, respectively. It can be seen from the profiles that the release process saturates well below 100%. The insets show the release kinetics at the beginning of the process.

release process well below 100% is a clear manifestation of the fact that solid-state diffusion of the dye inside the nanofibers is not involved (because diffusion can never stop below 100%).[36,37] Accordingly, the dye embedded in the nanofiber bulk cannot be released at all, and the only dye that is released is the one from the nanopore or the outer surfaces exposed to water.[36,37] The same is also true for the release of riboflavin, as illustrated in Figure 9a–e.

The release kinetics with the desorption-limiting stage is described by the following equation derived in refs 36 and 37

$$\frac{G_t}{M_{d0}} = \alpha\left[1 - \exp\left(\frac{-\pi^2}{8}\frac{t}{\tau_r}\right)\right] \quad (2)$$

dx.doi.org/10.1021/mp4003442 | *Mol. Pharmaceutics* 2013, 10, 4509–4526

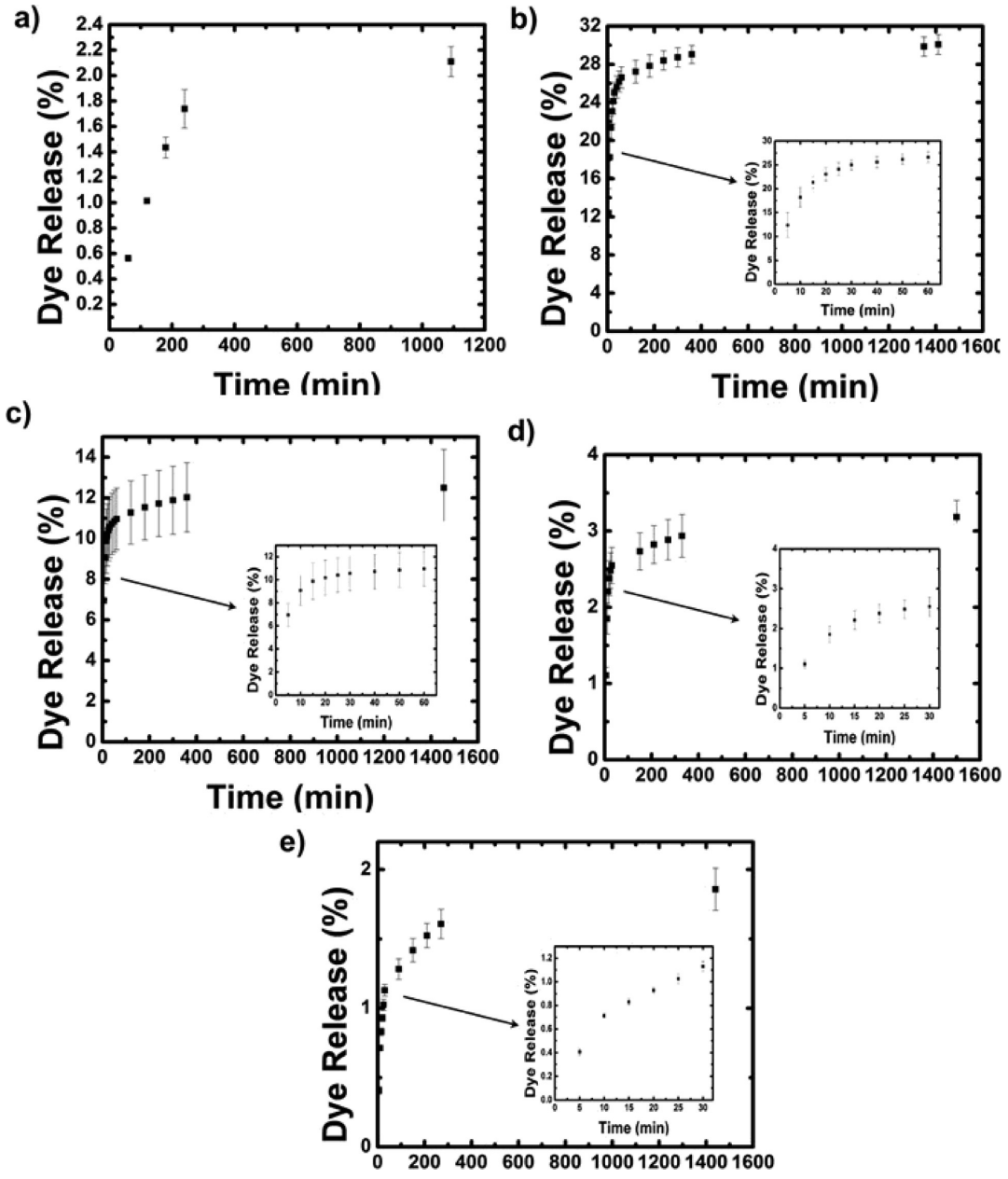

Figure 8. Release kinetics of Rhodamine B from electrospun PET-based nanofiber mats. Samples (a) I1, (b) J1, (c) K1, (d) L1, and (e) M1.

where G_t is the amount of dye released by time t, the nanoporosity factor $\alpha = M_{sd0}/(M_{sd0} + M_{bd0})$, with M_{sd0} being the initial amount of dye/drug at the nanopore surfaces, and M_{bd0} is the initial amount of dye/drug in the fiber bulk. Correspondingly, $M_{d0} = M_{sd0} + M_{bd0}$ is the total initial amount of dye/drug in the nanofibers. The nanoporosity factor is determined by polymer concentrations and molecular weights in the solutions. In eq 2, τ_r is the characteristic time of the release process, which is determined by the polymer density as well as the kinetic parameters of desorption, particularly by the pre-exponential k_0 and the activation energy E.[36,37] According to eq 2, dye/drug release should saturate at the level of $\alpha \times 100\%$.

It should be emphasized that the theory from refs 36 and 37 does not account for any dissolution of nanofibers during the release process and the exposition of the newly formed surfaces to the surrounding water. In other words, the original theory does not consider the presence of water-soluble soy protein, PEO, PVA, or PEG.[71] Moreover, the theory is applicable only to monolithic, single-polymer nanofibers. Therefore, the theory from refs 36 and 37 is not expected to describe the experimental data for the porogen-containing fibers and the core−shell fibers. Figure 10 shows the fit of eq 2 to the experimental data from the previous section. It clearly demonstrates that the inapplicable theory mostly fails to reproduce the data. The fitting yields the values of the nanoporosity factor and characteristic time and consequently the kinetic parameters of the desorption process, albeit in a very rough approximation. These parameters are listed in Table 2. It is emphasized that these values are mostly unreliable for the reasons described earlier. The table also incorporates several additional experimental parameters of interest: the release half-time, saturation rate, and saturation time. It is emphasized that the saturation rate in Table 3 yields only a rough estimate based on the maximum (plateau) release percentage and the saturation time, whereas the instantaneous release rate widely varies during the release process.

dx.doi.org/10.1021/mp4003442 | Mol. Pharmaceutics 2013, 10, 4509−4526

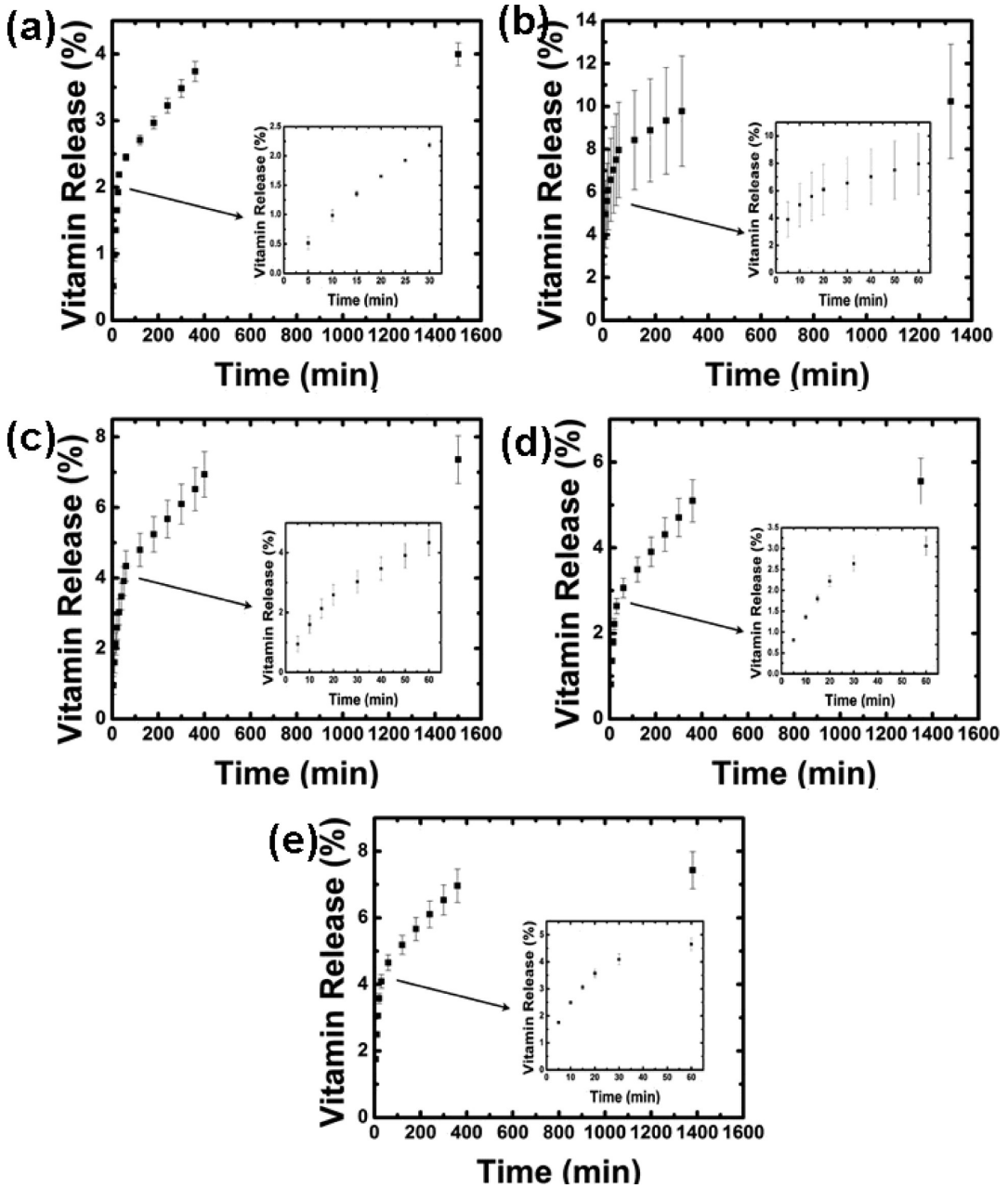

Figure 9. Release kinetics of riboflavin from electrospun PET-based nanofiber mats. Samples (a) I2, (b) J2, (c) K2, (d) L2, and (e) M2.

The comparison in Figure 10a shows that dye release from pure nylon 6 nanofiber mats cannot be fully described by eq 2. The latter stems from the following physicochemical factors. According to refs 72 and 73, nylon 6 partially swells in water. Water is absorbed in the amorphous regions by reacting with the free amide groups not bonded to the amide groups on the nearby chains or because of water breaking up the interaction between the chains. As nylon 6 swells in water, new nanopores are either generated or opened up. This factor is not accounted for by the theory in refs 36 and 37, which is an additional reason that it fails in practically all cases where nylon 6 is present in the fibers. It is emphasized that soy protein isolate is also partially soluble in water, as is seen in Table 1 (also, cf. ref 74). Therefore, soy-based nanofibers in contact with water dissolve to some extent, which results in the generation of new pores, a phenomenon not accounted for by the theory in refs 36 and 37, which is confirmed by the comparison in Figure 10.

Similar observations were done regarding the Rhodamine B-containing PET-based nanofiber mats. In particular, Figure 11 shows that the porogens (PEG and PEO) facilitated the release process and resulted in deviations from eq 2. The fitted rough values of the desorption parameters as well as some other experimental parameters of interest are listed in Table 3.

The release of riboflavin from the PET-based nanofibers follows the same trend (Figure 12 and Table 4). It is seen that in this case eq 2 is even less appropriate for fitting the data for the release kinetics as compared to the previously considered case of Rhodamine B release. This is probably linked to the fact that riboflavin is embedded in striations and develops microcracks during its release, as was discussed in relation to Figure 6. The development of microcracks is effectively identical to riboflavin acting as an additional autocatalytic self-porogen because it exposes more riboflavin to the surrounding bath during the release process.

dx.doi.org/10.1021/mp4003442 | *Mol. Pharmaceutics* 2013, 10, 4509−4526

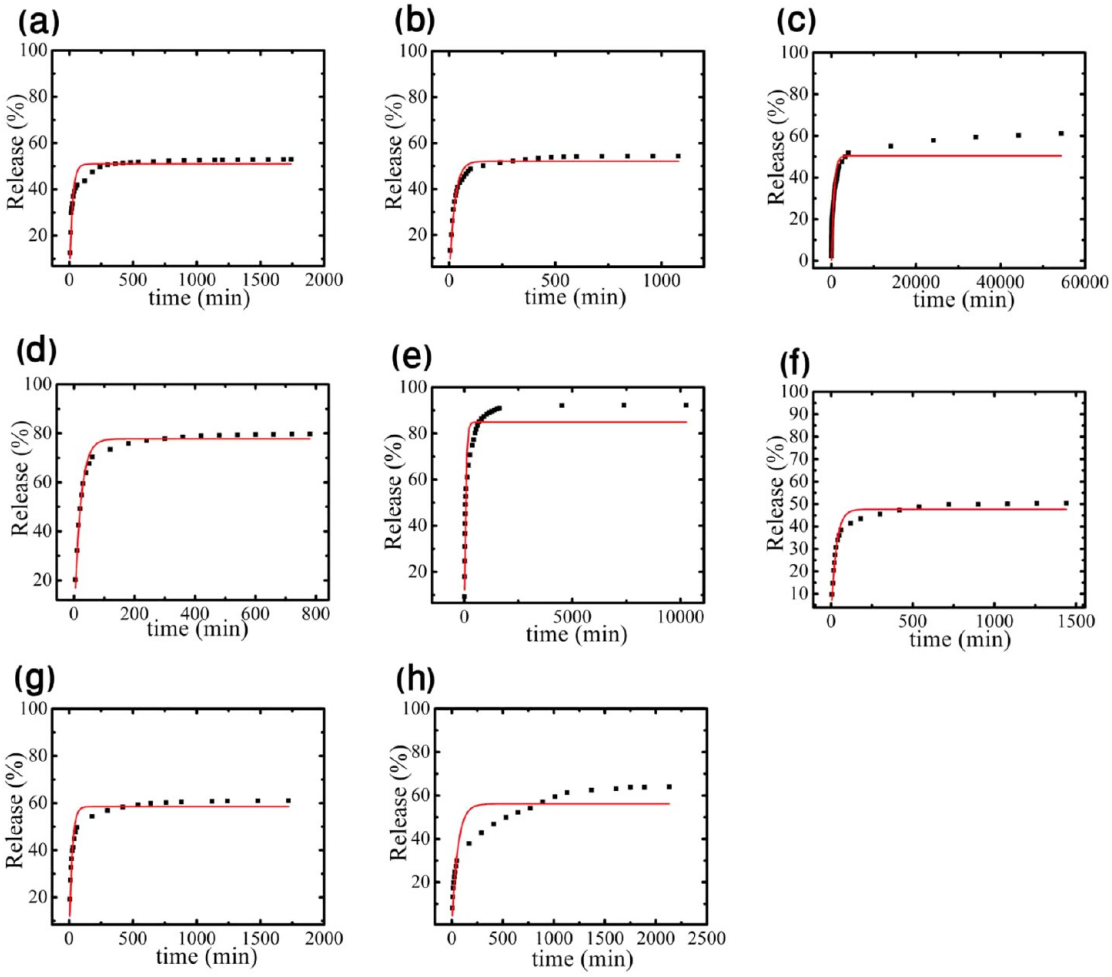

Figure 10. Experimental Rhodamine B release profiles versus eq 2. (a–h) Samples A–H from Figure 7a–h. The symbols show the experimental data, and the curves show the best fit of eq 2.

Table 2. Parameters of Equation 2 Determined from the Fitting in Figure 10[a]

	sample	average α (%)	average τ_r (min)	release half-time (min)	saturation time (min)	saturation rate (%/min)	average E (kJ/mol)
monolithic	nylon 6	55.30 ± 8.42	32.99 ± 5.78	40.58	300	0.17	30.37 ± 0.41
	SP/nylon	58.32 ± 4.49	31.49 ± 2.87	160	300	0.18	30.28 ± 0.2
	SP/PVA	62.12 ± 11.65	488.34 ± 177.76	3960	54 360	0.001	36.96 ± 0.95
	SP/nylon + 5% PEG	79.46 ± 3.59	27.71 ± 1.92	20	480	0.16	29.97 ± 0.17
	SP/nylon + 10% PEG	85.91 ± 0.94	74.58 ± 12.41	50	1270	0.07	32.42 ± 0.43
core–shell	SP/nylon	49.05 ± 2.65	35.44 ± 3.22	1080	1260	0.04	30.58 ± 0.23
	SP/nylon + 5% PEG	55.43 ± 3.98	37.12 ± 10.88	60	1480	0.04	30.61 ± 0.66
	SP/nylon + 10% PEG	57.15 ± 2.9	64.58 ± 23.77	530	1750	0.03	31.88 ± 1.07

[a]The values of α (%) show the ultimate release percentage, τ_r (min) is the characteristic time, and E (kJ/mol) is the desorption enthalpy.

Table 3. Parameters of Equation 2 Determined from the Fitting in Figure 11[a]

sample	average α (%)	release half-time (min)	saturation time (min)	saturation rate (%/min)	average τ_r (min)	average E (kJ/mol)
PET	2.14	120	950	0.002	208.29	23.59
PET/PEG	27.88	8.34	1090	0.028	12.8	28.05
PET/PEG/PEO 200 kDa	11.28	<5	1120	0.011	7.61	26.76
PET/PEG/PEO 400 kDa	2.87	8.34	1030	0.003	13.25	28.14
PET/PEG/PEO 600 kDa	1.53	20	1230	0.00151	25.35	29.76

[a]The values of α (%) show the ultimate release percentage, τ_r (min) is the characteristic time, and E (kJ/mol) is the desorption enthalpy.

The theory of ref 36, eq 2, can be amended by accounting for the fact that in the present case not only is dye released but also another water-soluble component, soy protein, PVA, or PEG, is being released as well as the riboflavin striations that result in

dx.doi.org/10.1021/mp4003442 | Mol. Pharmaceutics 2013, 10, 4509–4526

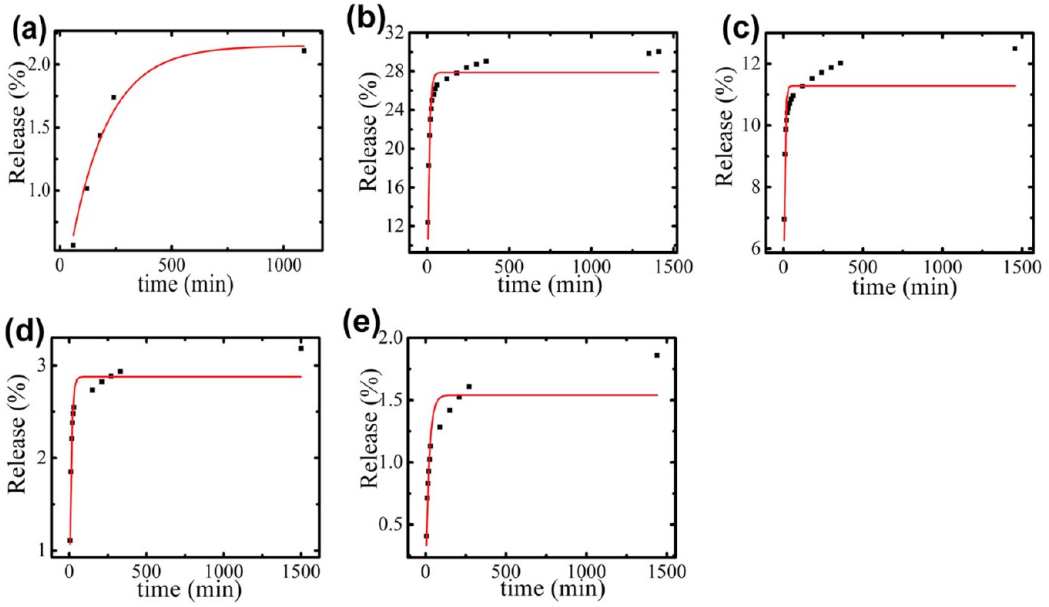

Figure 11. Release kinetics of Rhodamine B from samples I1−M1, which correspond to panels a−e in Figure 8, respectively. The symbols show the experimental data, and the curves show the best fit of eq 2.

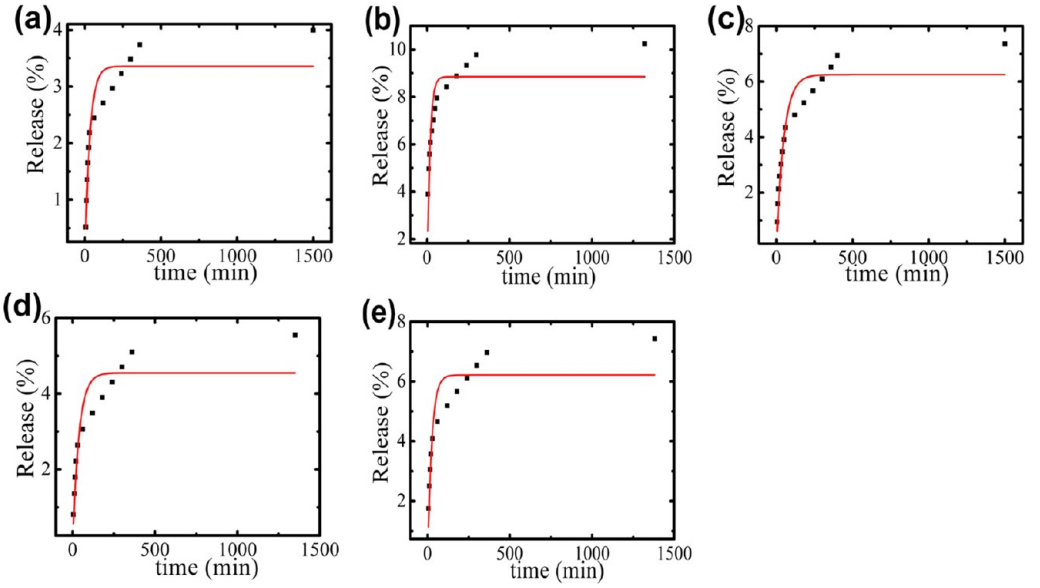

Figure 12. Release from riboflavin-loaded nanofiber mats (samples I2−M2), which correspond to panels a−e in Figure 9, respectively. The symbols show the experimental data, and the curves show the best fit of eq 2.

Table 4. Parameters of Equation 2 Determined from the Fitting in Figure 12[a]

sample	average α (%)	release half-time (min)	saturation time (min)	saturation rate (%/min)	average τ_r (min)	average E (kJ/mol)
PET	3.35	6.67	952	0.004	39.43	30.86
PET/PEG	8.85	11.43	1080	0.009	20.08	29.18
PET/PEG/PEO 200 kDa	6.24	44.81	850	0.009	59.5	31.88
PET/PEG/PEO 400 kDa	4.54	60	900	0.007	46.3	31.26
PET/PEG/PEO 600 kDa	6.21	26.85	1100	0.007	30.71	30.23

[a]The values of α (%) show the ultimate release percentage, τ_r (min) is the characteristic time, and E (kJ/mol) is the desorption enthalpy for the PET-based nanofiber mats with the embedded riboflavin.

microcracks and further exposure to the bath medium. Soy protein, PVA, and PEG are expected to be released much slower than the dye because of a much larger size of their molecules. Microcracks in the case of riboflavin release also form in the wake of the leading release process. Then, the additional dye or riboflavin release associated with the opening of the new pores or microcracks will proceed with the rate of release of the leachable component of the fibers or crack formation. Then, the dye/riboflavin

dx.doi.org/10.1021/mp4003442 | *Mol. Pharmaceutics* 2013, 10, 4509−4526

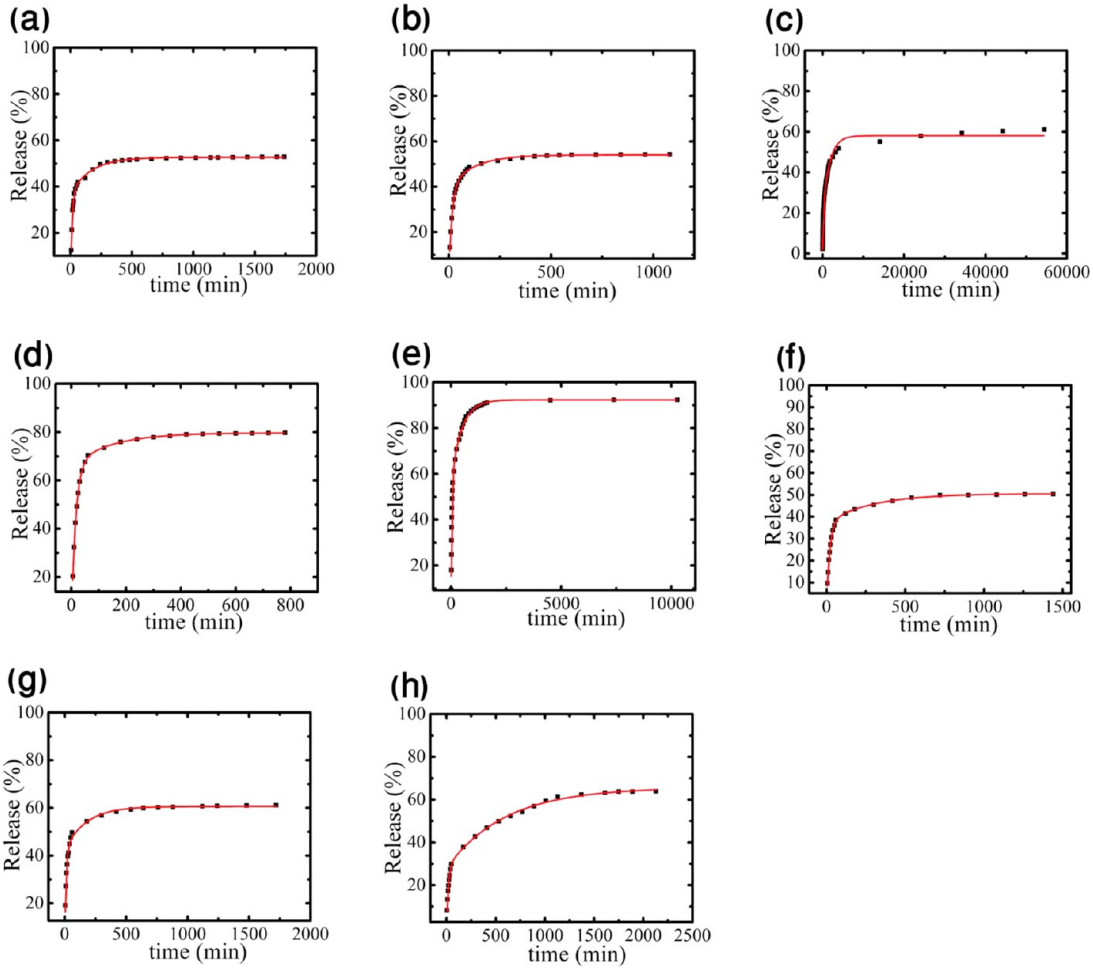

Figure 13. Experimental data for the dye (Rhodamine B) release kinetics from soy-protein-based nanofiber mat fitted using eq 3 for samples A–H, which correspond to panels a–h, respectively. The symbols show the experimental data, and the curves show the best fit of eq 3.

Table 5. Parameters of Equation 3 Determined from the Fitting in Figure 13 for Dye Release from Soy-Protein-Based Nanofiber Mats[a]

	sample	average α_1 (%)	average τ_{r1} (min)	average α_2 (%)	average τ_{r2} (min)	average E_1 (kJ/mol)	average E_2 (kJ/mol)
monolithic	nylon 6	38.21 ± 5.63	15.05 ± 2.35	20.17 ± 3.72	299.15 ± 97.95	28.43 ± 0.38	35.79 ± 0.6
	SP/nylon 6	49.23 ± 7.22	23.40 ± 3.46	10.79 ± 3.09	199.31 ± 40.66	29.53 ± 0.38	34.85 ± 0.26
	SP/nylon + 5% PEG	66.52 ± 3.84	20.55 ± 1.46	15.19 ± 1.24	191.58 ± 25.17	29.23 ± 0.17	34.78 ± 0.1
	SP/nylon + 10% PEG	56.80 ± 1.63	38.37 ± 6.56	36.77 ± 1.31	490.29 ± 180.73	30.75 ± 0.45	37.59 ± 0.04
core–shell	SP/nylon	36.98 ± 0.84	20.96 ± 2.71	15.66 ± 2.72	362.07 ± 14.04	29.26 ± 0.31	36.39 ± 0.02
	SP/nylon + 5% PEG	38.40 ± 3.98	13.67 ± 9.88	19.38 ± 1.16	396.03 ± 182.93	25.13 ± 5.6	36.31 ± 1.55
	SP/nylon + 10% PEG	30.41 ± 4.34	20.20 ± 7.21	33.94 ± 3.52	607.20 ± 132.24	29.00 ± 1.01	37.61 ± 0.34

[a]The values of α_i (%) show the ultimate release percentages of the dye and porogens, τ_{ri} (min), the characteristic times, and E_i (kJ/mol), the desorption enthalpies.

Table 6. Parameters of Equation 3 Determined from the Fitting in Figure 14 for Dye Release From PET-Based Nanofiber Mats[a]

sample	average α_1 (%)	average τ_{r1} (min)	average α_2 (%)	average τ_{r2} (min)	average E_1 (kJ/mol)	average E_2 (kJ/mol)
PET/PEG	24.77	5.13	9.54	235.96	25.77	35.32
PET/PEG/PEO 200 kDa	10.24	2.19	5.71	247.9	23.65	35.44
PET/PEG/PEO 400 kDa	2.58	0.62	10.27	519.61	20.50	37.29
PET/PEG/PEO 600 kDa	1.04	0.81	12.72	295.06	21.17	35.88

[a]The values of α_i (%) show the ultimate release percentages of the dye and porogens, τ_{ri} (min), the characteristic times, and E_i (kJ/mol), the desorption enthalpies.

dx.doi.org/10.1021/mp4003442 | *Mol. Pharmaceutics* 2013, 10, 4509–4526

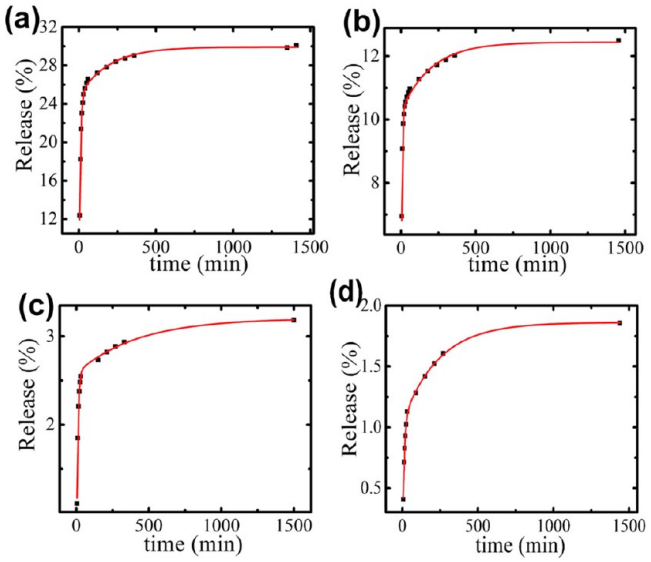

Figure 14. Experimental data on dye (Rhodamine B) release profiles from PET-based nanofiber mats fitted using eq 3 for samples J1−M1, correspond to panels a−d, respectively. The symbols show the experimental data, and the curves show the best fit of eq 3.

released by time t can be described by the superposition of the two terms dictated by eq 2

$$\frac{G_t}{M_{d0}} = \alpha_1\left[1 - \exp\left(-\frac{\pi^2}{8}\frac{t}{\tau_{r1}}\right)\right] + \alpha_2\left[1 - \exp\left(-\frac{\pi^2}{8}\frac{t}{\tau_{r2}}\right)\right] \quad (3)$$

where α_1 and τ_{r1} correspond to dye/riboflavin release from the existing pores and α_2 and τ_{r2} correspond to the release of a leachable component of the fibers or microcrack formation and thus to dye/riboflavin release from the surfaces of the newly formed pores/cracks.

According to ref 36, $\tau_{r1} = L^2/[Dc_{w01}b/\rho_{sd0}]$, where L is the pore length, D is the diffusion coefficient of dye in water, and the initial dye/riboflavin concentration in water near the pore surface is determined by $c_{w01} = k_{01}\exp(-E_1/RT)\,\rho_{sd0}/\rho_{sp}$, where k_{01} is the pre-exponential coefficient, E_1 is the desorption enthalpy of dye/riboflavin, R is the universal gas constant, T is the temperature, ρ_{sd0} is the surface concentration of dye/riboflavin at $t = 0$, and ρ_{sp} is the surface concentration of polymer matrix including the leaching polymer. Similarly, $\tau_{r2} = L^2/[Dc_{w02}b/\rho_{sl0}]$, where D is the diffusion coefficient of the leaching component in water (for simplicity, it is assumed to be the same as that for the dye) and the initial concentration of the leachable component in water near the pore surface is determined by $c_{w02} = k_{02}\exp(-E_2/RT)\rho_{sl0}/\rho_{spn}$, where k_{02} is the pre-exponential coefficient, E_2 is the desorption enthalpy of the leachable polymer, ρ_{sl0} is the surface concentration of the leachable component at $t = 0$, and ρ_{spn} is the surface concentration of the nonleachable polymer matrix. It is expected that release of dye by desorption is much easier than release of the leachable component because the latter has a much higher molecular weight. In the case of riboflavin, the role of the leachable polymer is also associated with riboflavin itself.

Figure 13 compares eq 3 with the same experimental data on dye release as in Figure 10. It can be seen that an almost perfect match is achieved, and the corresponding parameter values are listed in Table 5 for all of the samples in Figure 4 except

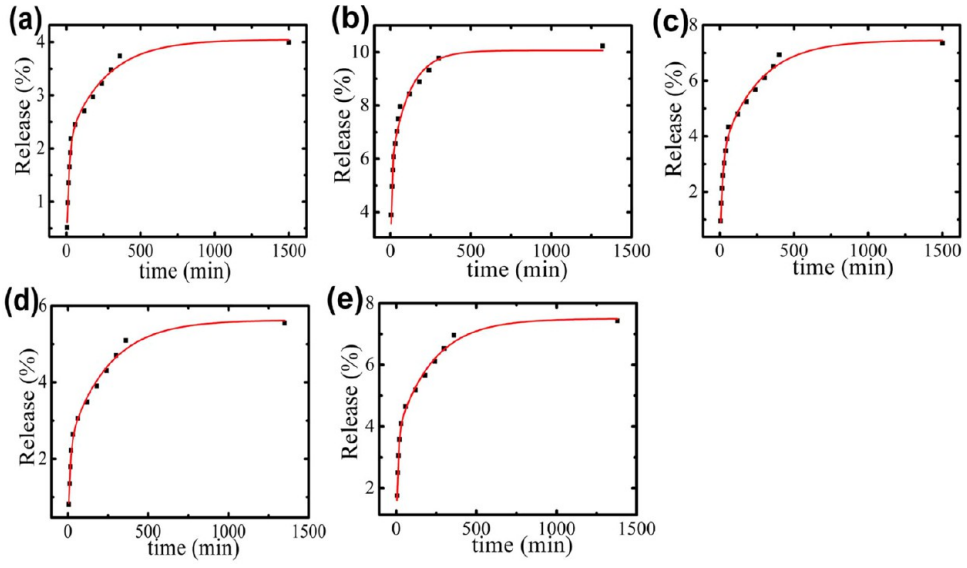

Figure 15. Experimental data on the riboflavin-release kinetics from the PET-based nanofiber mats fitted using eq 3 for samples I2−M2, which corresponding to panels a−e, respectively. The symbols show the experimental data, and the curves show the best fit of eq 3.

Table 7. Parameters of Equation 3 Determined from the Fitting in Figure 15 for the PET-Based Nanofiber Mats Releasing Riboflavin[a]

sample	average α_1 (%)	average τ_{r1} (min)	average α_2 (%)	average τ_{r2} (min)	average E_1 (kJ/mol)	average E_2 (kJ/mol)
PET	2.08	19.05	1.96	315.53	29.04	36.05
PET/PEG	5.7	6.82	4.35	142.78	26.48	34.07
PET/PEG/PEO 200 kDa	3.28	21.40	4.18	311.74	29.33	36.02
PET/PEG/PEO 400 kDa	2.33	15.14	2.33	303.87	28.47	35.95
PET/PEG/PEO 600 kDa	3.66	11.56	3.83	274.46	27.80	35.70

[a]The values of α_i (%) show the ultimate release percentages of riboflavin and porogens, τ_{ri} (min), the characteristic times, and E_i (kJ/mol), the desorption enthalpies.

dx.doi.org/10.1021/mp4003442 | Mol. Pharmaceutics 2013, 10, 4509−4526

for sample C. This soy/PVA nanofiber sample, as shown in Figure 4c2, lost its fibrillar structure and turned into a solid block owing to the dissolution of the constituents. This effect is not accounted for in the model (eq 3), and the agreement is poorer.

Figure 14 compares eq 3 with the experimental data on dye release from the PET-based nanofibers (samples J1−M1), whereas Figure 15 depicts a similar comparison with the experimental data on riboflavin release from the PET-based nanofibers (samples I2−M2). The corresponding parameter values are listed in Tables 6 and 7, respectively

■ CONCLUSIONS

Water-soluble fluorescent dye Rhodamine B was embedded in solution-blown soy protein/polymer monolithic and core−shell nanofiber mats, and the release kinetics from the samples submerged in water was studied experimentally. Similarly, release kinetics of Rhodamine B from PET-based electrospun nanofibers, and release kinetics of riboflavin (vitamin B_2) from PET-based electrospun nanofibers were explored. The main finding is that soy protein, PEO, PVA, and PEG embedded in nanofibers act as porogens and facilitate development of pores during the dye-release process, which affects the release kinetics. In addition, nylon 6 adsorbs water from the bath, which also affects the release kinetics.

Partially soluble riboflavin embedded in PET-based electrospun nanofibers is not dispersed uniformly but forms striations. During the release process, these striations facilitate the formation of microcracks, which means that riboflavin effectively acts as an autocatalytic self-porogen in addition to the other embedded porogens.

It was shown that the dye-release process from nanofiber mats with porogens or self-porogens is associated with the desorption-limited mechanism discovered in ref 36. The release process consists of two stages. In the first one, the dye/vitamin is released from the pre-existing pores, and in the second one, the dye/vitamin is released from the pores/microcracks formed as a result of leaching or dissolution of the fiber body or the generation of microcracks. The theory of ref 36 was amended appropriately to account for the two-stage character of the release process.

■ AUTHOR INFORMATION

Corresponding Author

*Tel.: +1 312 996 3472; Fax: +1 312 413-0447; E-mail: ayarin@uic.edu.

Author Contributions

⊥These authors contributed equally to this work.

Notes

The authors declare no competing financial interest.

■ ACKNOWLEDGMENTS

Parts of this work comprised a portion of the Ph.D. theses of S.K. and S.D. The work of S.K., S.S.R., A.L.Y., and B.P. was partially supported by a research contract with the United Soybean Board, Chesterfield, Missouri (research contract no. 0491). S.D. and A.H. were supported by The Scientific and Technological Research Council of Turkey (project no. 110M793), and the visit of S.D. to UIC was funded by The Council of Higher Education (Turkey).

■ REFERENCES

(1) Tuan, R. S.; Boland, G.; Tuli, R. Adult mesenchymal stem cells and cell-based tissue engineering. *Arthritis Res. Ther.* **2003**, *5*, 32−45.

(2) Caplan, A. I. Tissue engineering designs for the future: New logics, old molecules. *Tissue Eng.* **2000**, *6*, 1−8.

(3) Cancedda, R.; Dozin, B.; Giannoni, P.; Quarto, R. Tissue engineering and cell therapy of cartilage and bone. *Matrix Biol.* **2003**, *22*, 81−91.

(4) Li, W. J.; Tuli, R.; Huang, X.; Laquerriere, P.; Tuan, R. S. Multilineage differentiation of human mesenchymal stem cells in a three-dimensional nanofibrous scaffold. *Biomaterials* **2005**, *26*, 5158−5166.

(5) Ma, Z.; Kotaki, M.; Inai, R.; Ramakrishna, S. Potential of nanofiber matrix as tissue-engineering scaffolds. *Tissue Eng.* **2005**, *11*, 101−109.

(6) Liu, X.; Mai, P. X. Polymeric scaffolds for bone tissue engineering. *Ann. Biomed. Eng.* **2004**, *32*, 477−486.

(7) Pham, Q. P.; Sharma, U.; Mikos, A. G. Electrospinning of polymeric nanofibers for tissue engineering applications, a review. *Tissue Eng.* **2006**, *12*, 1197−1211.

(8) Sharma, B.; Elisseeff, J. H. Engineering structurally organized cartilage and bone tissues. *Ann. Biomed. Eng.* **2004**, *32*, 148−159.

(9) Khadka, D. B.; Haynie, D. T. Protein- and peptide-based electrospun nanofibers in medical biomaterials. *Nanomedicine* **2012**, *8*, 1242−1262.

(10) Price, R. L.; Gutwein, L. G.; Kaledin, L.; Tepper, F.; Webster, T. J. Osteoblast function on nanophase alumina materials: Influence of chemistry, phase, and topography. *J. Biomed. Mater. Res., Part A* **2003**, *67*, 1283−1295.

(11) Flemming, R. G.; Murphy, C. J.; Abrams, G. A.; Goodman, S. L.; Nealey, P. F. Effects of synthetic micro- and nano-structured surfaces on cell behavior. *Biomaterials* **1999**, *20*, 573−588.

(12) Wise, J. K.; Yarin, A. L.; Megaridis, C. M.; Cho, M. Chondrogenic differentiation of human mesenchymal stem cells on oriented nanofibrous scaffolds: Engineering the superficial zone of atricular cartilage. *Tissue Eng.* **2000**, *15*, 913−921.

(13) Fu, L.; Wang, W.; Yu, L.; Zhang, S.; Yang, G. Fabrication of novel cellulose/chitason artificial skin composite. *Mater. Sci. Forum* **2009**, *610−613*, 1034−1038.

(14) Laurencin, C. T.; Ambrosio, A. M. A.; Borden, M. D.; Cooper, J. A. Tissue engineering: Orthopedic applications. *Annu. Rev. Biomed. Eng.* **1999**, *1*, 19−46.

(15) Rosso, F.; Marino, G.; Giordano, A.; Barbarisi, M.; Parmeggiani, D.; Barbarisi, A. Smart materials as scaffolds for tissue engineering. *J. Cell. Physiol.* **2005**, *203*, 465−470.

(16) Li, W. J.; Danielson, K. G.; Alexander, P. G.; Tuan, R. S. Biological response of chondrocytes cultured in three dimensional nanofibrous poly(ε-caprolactone) scaffolds. *J. Biomed. Mater. Res., Part A* **2003**, *67*, 1105−1114.

(17) Li, W. J.; Tuli, R.; Okafor, C.; Derfoul, A.; Danielson, K. G.; Hall, D. J.; Tuan, R. S. A three-dimensional nanofibrous scaffold for cartilage tissue engineering using human mesenchymal stem cells. *Biomaterials* **2005**, *26*, 599−609.

(18) Jin, H. J.; Chen, J.; Karageorgiou, V.; Altman, G. H.; Kaplan, D. L. Human bone marrow stromal cell responses on electrospun silk fibroin mats. *Biomaterials* **2004**, *25*, 1039−1047.

(19) Boland, E. D.; Telemeco, T. A.; Simpson, D. G.; Wnek, G. E.; Bowlin, G. L. Utilizing acid pretreatment and electrospinning to improve biocompatibility of poly(glycolic acid) for tissue engineering. *J. Biomed. Mater. Res., Part B* **2004**, *71B*, 144−152.

(20) Matthews, J. A.; Wnek, G. E.; Simpson, D. G.; Bowlin, G. L. Electrospinning of collagen nanofibers. *Biomacromolecules* **2002**, *3*, 232−238.

(21) Boland, E. D.; Matthews, J. A.; Pawlowski, K. J.; Simpson, D. G.; Wnek, G. E.; Bowlin, G. L. Electrospinning collagen and elastin: Preliminary vascular tissue engineering. *Front. Biosci.* **2004**, *9*, 1422−1432.

(22) Kidoaki, S.; Kwon, K.; Matsuda, T. Mesoscopic spatial designs of nano- and microfiber meshes for tissue-engineering matrix and scaffold based on newly devised multilayering and mixing electrospinning techniques. *Biomaterials* **2005**, *26*, 37−46.

(23) Gombotz, W. R.; Pettit, D. K. Biodegradable polymers for protein and peptide drug delivery. *Bioconjugate Chem.* **1995**, *6*, 332−351.

(24) Verreck, G.; Chun, I.; Rosenblatt, J.; Peeters, J.; Van Dijck, A.; Mensch, J.; Noppe, M.; Brewster, M. E. Incorporation of drugs in an amorphous state into electrospun nanofibers composed of a water-insoluble, nonbiodegradable polymer. *J. Controlled Release* **2003**, *92*, 349−360.
(25) Kenawy, E. R.; Bowlin, G. L.; Mansfield, K.; Layman, J.; Simpson, D. G.; Sanders, E. H.; Wnek, G. E. Release of tetracycline hydrochloride from electrospun poly(ethylene-co-vinylacetate), poly(lactic acid), and a blend. *J. Controlled Release* **2002**, *81*, 57−64.
(26) Burgess, D. J.; Davis, S. S.; Tomlinson, E. Potential use of albumin microspheres as a drug delivery systems. I. Preparation and in vitro release of steroids. *Int. J. Pharm.* **1987**, *39*, 129−136.
(27) Robinson, J. R.; Lee, V. H. Influence of drug properties and routes of drug administration on the design of sustained and controlled release systems. In *Controlled Drug Delivery: Fundamentals and Applications*, 2nd ed.; Robinson, J. R., Lee, V. H. L., Eds.; Marcel Dekker: New York, 1987; pp 3−94.
(28) Fung, L. K.; Saltzman, W. M. Polymeric implants for cancer chemotherapy. *Adv. Drug Delivery Rev.* **1997**, *26*, 209−230.
(29) *Encyclopedia of Controlled Drug Delivery*; Leach, K. J., Mathiowitz, E., Eds.; Wiley: New York, 1999; Vol. *1*, pp 119−142.
(30) Gilding, D. K.; Reed, A. M. Biodegradable polymers for use in surgery polyglycolic/poly (lactic acid) homo and copolymers. *Polymer* **1979**, *20*, 1459−1464.
(31) Lewis, D. H. Controlled release of bioactive agents from lactide/glycolide polymers. In *Biodegradable Polymers as Drug Delivery Systems*; Chasin, M., Langer, R., Eds.; Marcel Dekker: New York, 1990; pp 1−8.
(32) Anderson, J. M.; Shive, M. S. Biodegradation and biocompatibility of PLA and PLGA microspheres. *Adv. Drug Delivery Rev.* **1997**, *28*, 5−24.
(33) Narasimhan, B. Mathematical models describing polymer dissolution: Consequences for drug delivery. *Adv. Drug Delivery Rev.* **2001**, *48*, 195−210.
(34) *Handbook of Pharmaceutical Controlled Release Technology*; Wise, D. L., Klibanov, A. M., Langer, R., Mikos, A. G., Peppas, N. A., Trantolo, D. J., Wnek, G. E., Yaszemski, M. J., Eds.; Marcel Dekker: New York, 2000.
(35) Langer, R.; Peppas, N. A. Advances in biomaterials, drug delivery, and bionanotechnology. *AIChE J.* **2003**, *49*, 2990−3006.
(36) Srikar, R.; Yarin, A. L.; Megaridis, C. M.; Bazilevsky, A. V.; Kelly, E. Desorption-limited mechanism of release from polymer nanofibers. *Langmuir* **2008**, *24*, 965−974.
(37) Gandhi, M.; Srikar, R.; Yarin, A. L.; Megaridis, C. M.; Gemeinhart, R. A. Mechanistic examination of protein release from polymer nanofibers. *Mol. Pharmaceutics* **2009**, *24*, 965−974.
(38) Huang, Z. M.; Zhang, Y. Z.; Kotaki, M.; Ramakrishna, S. A review on polymer nanofibers by electrospinning and their applications in nanocomposites. *Compos. Sci. Technol.* **2003**, *63*, 2223−2253.
(39) Moroni, L.; Licht, M.; Boer, J.; Wijn, J.; Blitterswijk, C. Fiber diameter and texture of electrospun PEOT/PBT scaffolds influence human mesenchymal stem cell proliferation and morphology, and the release of incorporated compounds. *Biomaterials* **2006**, *27*, 4911−4922.
(40) Nihant, N.; Grandfils, C.; Jerome, R.; Teyssie, P. Micro-encapsulation by coacervation of poly(lactide-co-glycolide) IV. Effect of the processing parameters on coacervation and encapsulation. *J. Controlled Release* **1995**, *35*, 117−125.
(41) Liao, I. C.; Chew, S. Y.; Leong, K. W. Aligned core-shell nanofibers delivering bioactive proteins. *Nanomedicine* **2006**, *1*, 465−471.
(42) Sinha-Ray, S.; Yarin, A. L.; Pourdeyhimi, B. The production of 100/400 nm inner/outer diameter carbon tubes by solution blowing and carbonization of core−shell nanofibers. *Carbon* **2010**, *48*, 3575−3578.
(43) Sinha-Ray, S.; Zhang, Y.; Yarin, A. L.; Davis, S.; Pourdeyhimi, B. Solution blowing of soy protein fibers. *Biomacromolecules* **2011**, *12*, 2357−2363.
(44) Khansari, S.; Sinha-Ray, S.; Yarin, A. L.; Pourdeyhimi, B. Stress-strain dependence for soy-protein nanofiber mats. *J. Appl. Phys.* **2012**, *111*, 044906-1−044906-13.
(45) *Paradigm for Successful Utilization of Renewable Resources*; Sessa, D. J., Willett, J. L., Eds.; AOCS Press: Champaign, IL, 1998.
(46) Morrison, M.; Shah, Y.; Ustynoski, A.; Wolak, K. *Bioadsorbable soy sutures*; Purdue University Agricultural and Biological Engineering Senior Capstone Projects: West Lafayette, IN, 2012. https://engineering.purdue.edu/ABE/InfoFor/CurrentStudents/SeniorProjects/2012/MorrisonShahUstynoskiWolak.
(47) Duzyer, S.; Hockenberger, A.; Zussman, E. Characterization of solvent-spun polyester nanofibers. *J. Appl. Polym. Sci.* **2011**, *120*, 759−769.
(48) Veleirinho, B.; Rei, M. F.; Lopes-da-Silva, J. A. Solvent and concentration effects on the properties of electrospun poly(ethylene terephthalate) nanofiber mats. *J. Polym. Sci., Part B: Polym. Phys.* **2008**, *46*, 460−471.
(49) Whelove, O. E.; Cozad, M. J.; Lee, B. D.; Sengupta, S.; Bachman, S. L.; Ramshaw, B. J.; Grant, S. A. Development and in vitro studies of a polyethylene terephthalate-gold nanoparticle scaffold for improved biocompatibility. *J. Biomed. Mater. Res., Part B* **2011**, *99B*, 142−149.
(50) Ma, Z.; Kotaki, M.; Yong, T.; Wei, H.; Ramakrishna, S. Surface engineering of electrospun polyethylene terephthalate (PET) nanofibers towards development of a new material for blood vessel engineering. *Biomaterials* **2005**, *26*, 2527−2536.
(51) Ramires, P. A.; Mirenghi, L.; Romano, A. R.; Palumbo, F.; Nicolardi, G. Plasma-treated PET surfaces improve the biocompatibility of human endothelial cells. *J. Biomed. Mater. Res.* **2000**, *51*, 535−539.
(52) Trail, I. A.; Powell, E. S.; Noble, J. An evaluation of suture materials used in tendon surgery. *J. Hand Surg.* **1989**, *14*, 422−427.
(53) Viinikainen, A.; Goransson, H.; Huovinen, K.; Kellomaki, M.; Tormala, P.; Rokkanen, P. Material and knot performances of braided polyester (Ticron) and bioabsorbable poly-L/D-lactide (PLDA) 96/4 sutures. *J. Mater. Sci.* **2006**, *17*, 169−177.
(54) Amis, A. A.; Kempson, S. A.; Campbell, J. R.; Miller, J. H. Anterior cruciate ligament replacement. *J. Bone Jt. Surg.* **1988**, *70B*, 628−634.
(55) Andrzejak, S.; Fourtuniak, J.; Wrobel-Wisniewska, G.; Zawirski, M. Clinical evaluation of the polypropylene-polyester knit used as a cranioplasty material. *Acta Neurochir.* **2005**, *147*, 973−976.
(56) Nair, P. D.; Sreenivasan, K.; Jayabalan, M. Multiple gamma radiation sterilization of polyester fibres. *Biomaterials* **1988**, *9*, 335−338.
(57) Pillai, O.; Panchagnula, R. Polymers in drug delivery. *Curr. Opin. Chem. Biol.* **2001**, *5*, 337−470.
(58) Xu, X.; Chen, X.; Wang, Z.; Jing, X. Ultrafine PEG-PLA fibers loaded with both paclitaxel and doxorubicib hydrochloride and their in vitro cytotoxicity. *Eur. J. Pharm. Biopharm.* **2009**, *72*, 18−25.
(59) Ranganath, S. H.; Wang, C. H. Biodegredable microfiber implants delivering paclitaxel for post-surgical chemotherapy against malingnant glioma. *Biomaterials* **2008**, *29*, 2996−3003.
(60) Xie, L.; Tan, R. S.; Wang, C. H. Biodegredable microparticles and fiber fabrics for sustained delivery of cisplatin to treat C6 glioma in vitro. *J. Biomed. Mater. Res., Part A* **2008**, *85*, 897−908.
(61) Stammen, J. A.; Williams, S.; Ku, D. N.; Guldberg, R. E. Mechanical properties of a novel PVA hydrogel in shear and unconfined compression. *Biomaterials* **2001**, *22*, 799−806.
(62) Ethicon Nylon Suture. http://www.ethicon360.com/products/ethilon-nylon-suture.
(63) Lembach, A.; Tan, H. B.; Roisman, I. V.; Gambaryan-Roisman, T.; Zhang, Y.; Tropea, C.; Yarin, A. L. Drop impact, spreading, splashing and penetration in electrospun nanofiber mats. *Langmuir* **2010**, *26*, 9516−9523.
(64) Zhang, Y.; Yarin, A. L. Stimuli-responsive copolymers of N-isopropyl acrylamide with enhanced longevity in water for micro- and nanofluidics, drug delivery and non-woven applications. *J. Mater. Chem* **2009**, *19*, 4732−4739.

(65) de Gennes, P. G.; Brochard-Wyart, F.; Quere, D. *Capillarity and Wetting Phenomena: Drops, Bubbles, Pearls, Waves*; Springer, New York, 2004.
(66) Sinha-Ray, S.; Khansari, S.; Yarin, A. L.; Pourdeyhimi, B. Effect of chemical and physical cross-linking on tensile characteristics of solution-blown soy protein nanofiber mats. *Ind. Eng. Chem. Res.* **2012**, *51*, 15109−15121.
(67) Casper, C. L.; Stephens, J. S.; Tassi, N. G.; Chase, D. B.; Rabolt, J. F. Controlling surface morphology of electrospun polysterene fibers: Effect of humidity and molecular weight in the electrospinning process. *Macromolecules* **2004**, *37*, 573−578.
(68) Dror, Y.; Salalha, W.; Avrahami, R.; Zussman, E.; Yarin, A. L.; Dersch, R.; Greiner, A.; Wendorff, J. H. One-step production of polymeric micro-tubes via co-electrospinning. *Small* **2007**, *3*, 1064−1073.
(69) Zussman, E.; Yarin, A. L.; Bazilevsky, A. V.; Avrahami, R.; Feldman, M. Electrospun polyacrylonitrile/poly(methyl methacrylate)-derived carbon micro-/nanotubes. *Adv. Mater.* **2006**, *18*, 348−353.
(70) Sinha- Ray, S.; Zhang, Y.; Placke, D.; Megaridis, C. M.; Yarin, A. L. Resins with nano-raisins. *Langmuir* **2010**, *26*, 10243−10249.
(71) Mark, J. E. *Polymer Data Handbook*; Oxford University Press: New York, 1999.
(72) Inoue, K.; Hoshino, S. Swelling of nylon 6 film due to water sorption. *J. Polym. Sci.* **1976**, *14*, 1513−1526.
(73) Kawasaki, K.; Sekita, Y.; Kanou, K. The extension of nylon 6 as a function of the extent and nature of sorbed water. *J. Colloid Sci.* **1962**, *17*, 865−871.
(74) *PRO-FAM 955 Isolated Soy Protein 066-955*; Data Sheet from ADM Specialty Products-Oilseeds: Decatur, IL.